Global Particle Simulation for a Space Weather Model: Present and Future

K.-I. Nishikawa, S. Ohtani

K.-I. Nishikawa, Department of Physics and Astronomy, Rutgers, The State University of New Jersey, 136 Frelinghuysen Road, Piscataway, NJ 08854-8019. E-mail: kenichi@physics.rutgers.edu.

S. Ohtani, The Johns Hopkins University, Applied Physics Laboratory, Johns Hopkins Road, Laurel, MD 20723-6099. E-mail: ohtani@fluxgate.jhuapl.edu.

Abstract

We report progress in the long-term effort to represent the interaction of the solar wind with the Earth's magnetosphere using a three-dimensional electromagnetic particle model (EMPM) as a Space Weather Model. MHD simulation models have been refined to establish quantitative global modeling in comparison with observations. The EMPM has become more feasible as the power and speed of supercomputers have improved in recent years.

Simulations with southward and dawnward turning IMFs have revealed the fundamental processes which have been confirmed by MHD simulations and observations. After a quasi-steady state is established with an unmagnetized solar wind, a southward IMF is switched on, which causes the magnetosphere to stretch with reconnection at the dayside magnetopause. The plasma sheet in the near-Earth magnetotail clearly thins. The cross-field current also thins and intensifies, which excites a kinetic (drift kink) instability along the dawn-dusk direction. As a result of this instability the electron compressibility effect appears to be reduced and to allow the collisionless tearing to grow rapidly with the reduced B_z component. Later, magnetic reconnection also takes place in the near-Earth magnetotail.

In the case where the northward IMF is switched gradually to dawnward, magnetic reconnection takes place at both the dawnside and duskside. The arrival of dawnward IMF at the magnetopause creates a reconnection groove which causes particle entry into the deep region of the magnetosphere via field lines that go near the magnetopause. The flank weak-field region joins onto the plasma sheet and the current sheet to form a geometrical feature called the cross-tail S that structurally integrates the magnetopause and the tail interior. This structure might contribute to direct entry of the magnetosheath plasma to the plasma sheet, in which the entry process heats the magnetosheath plasma to plasma sheet temperatures.

In spite of the coarseness of the simulations, the EMPM can reproduce some of the basic physics involved in the solar wind-magnetosphere interaction. Furthermore, kinetic processes included in particle simulations have revealed the essential physics involved in the substorm onset. Based on present progress, the EMPM will provide further understanding of the fundamental physical processes, in particular of substorm and storm onsets and of energetic particle injection into the inner magnetosphere and ionosphere with further improvement in resolutions and plasma parameters. Considering the performance of EMPM in tracing particles from the solar wind through and into the magnetosphere, it seems likely that EMPM will play an important role in predicting the storm onset and its intensity in the near future.

I. Introduction

The interaction of the solar wind with the Earth's magnetic field gives rise to a number of important and intriguing phenomena, many of which are only partially understood. These include reconnection between the solar wind magnetic field and geomagnetic field lines at the dayside magnetopause (including patchy plasma transfer), reconnection in the magnetotail, plasma convection in the magnetosphere/ionosphere, generation of field-aligned current systems, and energetic particle injection. A wide range of physical processes is involved in the solar wind-magnetosphere system, and consequently a wide array of methods has been used to study them, ranging from detailed studies of select phenomena with the assumption of a specific field geometry or boundary conditions, to fully three-dimensional simulations with MHD assumptions.

MHD simulations have progressed intensively in their numerical methodology and their physics since the first 2-D MHD simulation of the magnetosphere was developed [1]. In MHD codes the microscopic processes can be represented by statistical (macroscopic) parameters such as diffusion coefficients, anomalous resistivity, viscosity, temperature, and the adiabatic constant in the equation of state (see the articles by Gombosi et al. [2] and Clauer et al. [3] in this issue for reviews of MHD simulations). Recently, the Hall term in the generalized Ohm's law has been identified as playing an important role in controlling the reconnection rate in collisionless plasmas [4]. Based on this idea, a new simulation model has been developed incorporating a higher-order form of Ohm's law which retains corrections of the order of the ion skin depth (the electrons are assumed to be in steady-state or approximate thermal equilibrium, due to their rapid motion along the field lines) [5]. The near-Earth magnetotail is one of the regions where kinetic effects are critical and particle simulations become essential [6], [7].

Since the strong coupling between the solar wind and the magnetosphere during the southward IMF phase of the cloud allows a significant fraction of the incident solar-wind kinetic energy to enter the magnetosphere [8], reconnection in the magnetotail will be reviewed briefly (for details, see the articles by Pritchett [9] and Hesse [10] in this issue). Certainly, solar winds with both an enhanced density and a southward IMF will lead to more complicated and drastic phenomena than solar winds with only a southward IMF

[11], [12]. Because of the importance of magnetic reconnection in the near-Earth magnetotail, theories and simulations with various methods have been performed extensively. The tearing instability in the magnetotail has been studied [13], [14]. The collisionless tearing instabilities are stabilized due to electron adiabaticity with a finite B_z component, which causes free energy otherwise available for the instability to be used up by plasma compression [15], [16], [17], [18]. Two-dimensional local particle simulations show the formation of a thin current sheet with a deep minimum in the equatorial B_z field in the near-Earth magnetotail and with the inductive electric field carried by a southward IMF [19]. In the Geospace Environmental Modeling (GEM) Reconnection Challenge project, the evolution of a simple Harris sheet has been explored with a broad variety of codes, ranging from fully electromagnetic particle in cell (PIC) codes to conventional resistive magnetohydrodynamic (MHD) code [20] (and the accompanying papers). The key conclusion of the project is that the Hall effect is the critical factor that must be included to model collisionless reconnection.

Recent 3-D particle simulations indicate that the collisionless tearing instability grows rapidly due to the reduction of electron compressibility caused by the persistent drift kink mode (not included in single-fluid treatments) in the presence of a small B_z component [7], [21], [22]. Furthermore, Pritchett and Coroniti [23] have shown that highly east-west structured strong plasma flows can develop within the convectively-driven plasma sheet due to the combined dynamical effects of reconnection and unstable drift kink modes for the case where no magnetic flux is allowed into the system. As will be described later, global simulations [11], [12] show this highly east-west structured strong plasma flow. These global simulations include effects from the dayside magnetopause, a self-consistent magnetic field stretched by the solar wind with an IMF in the magnetotail, and particle entry from low-latitude boundary layers on the flanks (especially in the presence of an IMF B_y component) [24], [25]. They are important for the magnetotail dynamics [26], [27]. Based on the previous work, at the present time the drift-kink-mode instability [11], [12], [28], [29] seems to be a candidate for the cross-field streaming instability; however, further investigation is necessary with larger mass ratios.

By investigating the sources of the particles in the inner magnetosphere, one can get a

better understanding of the processes that control the injection and heating of particles in the magnetosphere. Changes in the solar wind conditions drive substorms and storms. but these phenomena are difficult to understand because a variety of processes, regions, and scale lengths are involved. In the following sections, we will discuss how studies using the EMPM have provided significant insight into the triggering processes of substorms. This model makes major advances in that the electron and ion motions are incorporated separately and each species is diagnosed according to the physics involved. Through the separation of the electron and ion dynamics, a more physical picture of magnetic reconnection and substorms is attained and can be tested against observations.

In principle the EMPM enables us to investigate the global simulation of the solar wind interaction with an IMF including the complete particle physics. As will be shown below, the advantage is that the basic equations of the model contain the complete physics. The price to be paid is that, with present supercomputers, the plasma parameters must be scaled and the resolutions in space and time are coarse. In the next section the EMPM is described. In section 3 the simulation results with southward turning IMF are reviewed including the substorm onset. The simulation results with dawnward turning IMF after northward IMF exhibit a reconnection groove in the dawnside and duskside magnetopause, which facilitates particle entry into the inner magnetosphere. The present status and future development and perspective goals of EMPMs as a Space Weather Model are discussed in association with the scientific goals of future missions such as Cluster II, the Magnetospheric Multiscale Mission, and the Magnetotail Constellation, Dynamics, Reconnection, And Configuration Observatory (DRACO).

II. Three-Dimensional Electromagnetic Particle Simulation Model (EMPM)

Our code is a successor to the TRISTAN code [30]. Its new features [31] are (1) Poisson's equation and Fourier transforms have been eliminated by updating the fields locally from the curl equations and depositing the particle currents according to charge-conserving formulas [32], (2) radiative boundary conditions are applied to the fields using a first-order Lindman approximation [33], (3) filtering is done locally, (4) localization makes the code ideally suited to modern parallel machines which call for minimizing data paths, (5)

the code is in FORTRAN and fully transportable: modest versions run on PCs and on workstations. The new version of the code has been applied to the study of the dynamics of low-β plasma clouds [34], the whistler waves driven by the Spacelab-2 electron beam [35], [36], and the coalescence of two current loops [37], [38], [39].

For the simulation of solar wind-magnetosphere interactions the following boundary conditions were used for the particles [11], [12], [24], [40], [41], [42]: (1) Fresh particles representing the incoming solar wind were continuously injected across the $y - z$ plane at $x = x_{min}$ with a thermal velocity plus a bulk velocity in the $+x$ direction; (2) a thermal solar particle flux was also injected across the sides of their rectangular computation domain; (3) escaping particles were arrested in a buffer zone, redistributed there more uniformly by making the zone conducting in order to simulate their escape to infinity, and were finally written off. The EMPM used a simple model for the ionosphere in which both electrons and ions were reflected by the Earth's dipole magnetic field. The effects of a conducting ionospheric boundary will be developed in future simulations. The effects of the Earth's rotation were not included.

For the fields, boundary conditions were imposed just outside these zones [11], [12], [24], [40], [41]: radiation was prevented from being reflected back inward, following Lindman's ideas [33]. The lowest-order Lindman approximation was found adequate: radiation at glancing angles was no problem. However, special attention was given to conditions on the edges of the computational box.

In order to bring the naturally disparate time scale and space scale closer together in this simulation of phenomena dominated by ion inertia and magnetic field interaction, the electron mass was raised to 1/16 of the ion mass and the velocity of light was lowered to twice the incoming solar wind velocity. This means that charge separation and kinetic phenomena were included qualitatively but perhaps not with quantitative accuracy. Likewise, radiation-related phenomena (e.g., whistler mode waves) were included qualitatively.

III. Simulation Results

Solar wind with no IMF

The first test exploring the solar wind-magnetosphere interaction with an unmagnetized

solar wind was run on the CRAY-YMP at NCAR using a modest 105 by 55 by 55 grid and only 200,000 electron-ion pairs [40]. Buneman et al. [41] have also reported on their second test run on the CRAY-2 at NCSA using a larger 215 by 95 by 95 grid and about 1,500,000 electron-ion pairs. Initially, these fill the entire box uniformly and drift with a velocity $v_{sol} = 0.5c$ in the $+x$ direction, representing the solar wind without an IMF. The electron and ion thermal velocities are $v_{et} = (T_e/m_e)^{1/2} = 0.2c$, and $v_{it} = (T_i/m_i)^{1/2} = 0.05c\,(= v_s = (T_e/m_i)^{1/2})$, respectively, while the magnetic field is initially zero. A circular current generating the dipole magnetic field is increased smoothly from 0 to a maximum value reached at time step 65 and kept constant at that value for the rest of the simulation. The center of the current loop is located at $(70.5\,\Delta,\ 47.5\,\Delta,\ 48\,\Delta)$ with the current in the $x-y$ plane and the axis in the z direction. The initial expansion of the magnetic field cavity is found to expel a large fraction of the initial plasma. The injected solar wind density is about 0.8 electron-ion pairs per cell, the mass ratio is $m_i/m_e = 16$, and $\omega_{pe}\Delta t = 0.84$. In the simulations reported in this paper the grid spacing Δ corresponds to approximately $1 R_{\mathrm{E}}$ (The distance between the dayside magnetopause and the Earth in the simulations is about $10\,\Delta$). The time step in the simulations corresponds to about 10 seconds on the basis of the solar wind velocity, the corresponding distance, and the mass ratio (Due to the heavy electrons the MHD phenomena seem react fast). Time step 1152 in the simulation is set at 0.00 UT to provide a sense of relative time frame in the simulations (1088; -00.10 UT: 1152; 00.00 UT: 1216; 00.10 UT: 1280; 00.20 UT: 1344; 00.30 UT: 1408; 00.40 UT: 1472; 00.50UT).

Southward turning IMF

At step 768 $(-1.00$ UT$)$ [41], [42], a southward IMF $(B_z^{IMF} = -0.4)$ is switched on at $x = 66\,R_{\mathrm{E}}$, and the solar wind with the southward IMF reaches about $x = 120\,\Delta (= -50\,R_{\mathrm{E}})$ at step 1280 (0.20 UT). The Alfvén velocity with this IMF is $v_A/c = 0.1(\bar{n}_i)^{-1/2} = 0.1$ for the average ion density $\bar{n}_i = 1$.

Figure 1 shows the electron density in the noon-midnight meridian $(x - z)$ plane containing the Earth $((x, y) = (70\,\Delta,\ 48\,\Delta))$ at 0.10 UT (1216) (a); 0.20 UT (1280) (b); 0.30 UT (1344) (c); and 0.40 UT (1408) (d) with the southward IMF (The maximum electron density is normalized to the same value for all panels so that comparisons can be made

easily.). The electron density is color coded and the magnetic field component in the plane is shown with arrows at every third grid point. The magnitude of the field has been scaled so as to make the field direction clearer for weak fields, so the length of the vectors is not a true representation of the field magnitude. The solar-wind particles flow from left to right. The dipole field is compressed on the side facing the solar wind and is extended to a long tail on the downwind side, just as the Earth's magnetic field is in the solar wind [40], [41], [42], [11], [12], [24]. More particles penetrate into the magnetotail near the Earth in the case of southward IMF, as shown in Fig. 1, than in the case with no IMF, as shown by Nishikawa et al. [42]. This is attributable to magnetic reconnection at the dayside magnetopause [43], [44], [45], [46]. As shown in [11], at 0.10 UT (1216) the near-Earth magnetotail clearly thins, a tearing instability starts to grow near $x = 85\,\Delta (= -15\,R_{\mathrm{E}})$, and the density is bunched in the magnetotail owing to this instability as shown in Fig. 1b. At 0.30 UT (1344) (Fig. 1c) electrons are evacuated from the reconnection region as found in an earlier simulation [21].

To display magnetic reconnection at the dayside magnetopause and in the magnetotail, Figure 2 shows the magnetic field lines in the noon-midnight meridian plane at four different times. (Geocentric solar magnetospheric (GSM) coordinates are used only in Figures 2 and 10.) At -0.20 UT (1024), the solar wind with its southward IMF starts to interact with the dipole magnetic field at the dayside magnetopause (Fig. 2a). Figure 2b shows the X-point at the magnetopause at -0.10 UT (1088) [44]. The southward IMF is bent by the magnetosphere as shown in Figure 2c at 0.10 UT (1216). Figure 2c displays an interesting magnetic structure near the subsolar magnetopause. Three-dimensional analysis shows that the reconnection occurs three-dimensionally in the dayside magnetopause along the equator (see, for example, [47]). At the same time stretched dipole magnetic fields are observed, particularly in Figure 2c. Furthermore, the magnetic fields are stretched in the magnetotail, which leads to the growth of a tearing instability there. Figure 2d shows magnetic reconnection occurring at 0.20 UT (1280), with the X-point located near $x = 85\,\Delta\ (= -15\,R_{\mathrm{E}})$ [21].

Dipolarization is one of the processes that is closely related to the generation of wedge currents [48], [49]. The total magnetic field strength $|\mathbf{B}(x, y, z)|$ at $y = 47\,\Delta$) in the

noon-midnight $(x - z)$ plane in the near-Earth magnetotail is plotted on a logarithmic scale at 0.00 UT (1152) (a), 0.10 UT (1216) (b), 0.20 UT (1280) (c), and 0.30 UT (1344) (d) in Fig. 3 [50]. In these figures the maximum and minimum values are set so as to highlight the changes due to reconnection and to the dipolarization of the magnetotail. The arrows represent the magnetic field (scaled to show the weaker fields). At 0.00 UT (1152) (Fig. 3a) the arrows show an ordinary stretched dipole magnetic field. Further stretching of the magnetic field is found in the weakening normal component (B_z) (still positive) in the central plasma sheet (Fig. 3b). At 0.20 UT (1280) an X-point is created, marking the occurrence of reconnection around $x = 85\,\Delta(= -15R_E)$ as shown in Fig. 3c. Due to the reconnection the normal (z) components become negative $(83 < x/\Delta < 90)$ in the central sheet. At the same time local dipolarization is found around $x = 80\,\Delta$ (it is more easily recognized with a vertical line at $x = 80\,\Delta(= -10\,R_{\rm E})$. The contour curve at the value -0.4 (light green-yellowish green) moves tailward at 0.20 UT (1280). This comes partially from the magnetic field transfer by the earthward flows generated by the reconnection. Further dipolarization takes place in the near-Earth magnetotail as shown in Fig. 3d. The evidence for dipolarization is subtle, therefore careful attention is needed to recognize it, and this can be done in two ways. Firstly, the weak magnetic field region (in dark blue) created by the reconnection around $(x, z) = (82\,\Delta, 48\,\Delta)$ in Fig. 3c moves tailward by $2\,R_{\rm E}$ in Fig. 3d $((x, z) = (84\,\Delta, 48\,\Delta))$. Secondly, the negative B_z components on the subsolar line $(z = 48\,\Delta)$ $(83 \leq x/\Delta \leq 85)$ (Fig. 3c) become positive in Fig. 3d (this is viewed easily using magnification by acroread (Acrobat Reader) at http://www.physics.rutgers.edu/ kenichi). Furthermore, detailed analysis shows that the contour curve at the value 0.200 (yellow-yellowish green) which is bowed toward the Earth at the subsolar line (Fig. 3c) becomes more straight (less bowed) due to the dipolarization in Fig. 3d (this is seen more easily by drawing a vertical line at $x = 79\,\Delta$). As will be shown in Fig. 5, the dipolarization coincides with the current decrease at 0.30 UT (1344).

The magnetic reconnection takes place around $x = 85\,\Delta(= -15\,R_{\rm E})$ (see Fig. 2d). The tearing instability is excited by the combined effects of the reduced B_z and the kinetic (drift kink) instability along the dawn-dusk direction. The identification of this instability requires further investigation with larger mass ratios and better resolutions. In order to

confirm that the kinetic instability is excited along the y (dawn-dusk) direction, the time evolution of the plasma sheet is examined in the dawn-dusk plane at $x = -15\,R_{\mathrm{E}}$. [12]. Figure 4 shows the electron density on the dawn-dusk $(y-z)$ plane with the magnetic field (B_y, B_z) represented by arrows at 0.00 UT (1152) (a), 0.10 UT (1216) (b), 0.20 UT (1280) (c), and 0.30 UT (1344) (d) (viewed from further down the tail). The north and south lobes appear in dark blue (low density) and are surrounded by the magnetopause. The magnitude of the field has been scaled so as to make the field direction clearer for weak fields, so the length of the vectors is not a true representation of the field magnitude. As shown in Fig. 4a and 4b, the plasma sheet is kinked as found in localized 3-D simulations [7], [21], [51], [52]. This structure is similar to Fig. 3 in [53]. The electron compressibility effect appears to have decreased due to the transport of plasma across flux tubes caused by the drift kink instability [7], [11], [12], [21]. Consequently, the tearing instability grows rapidly. The northward closed magnetic field (see Fig. 4a) is disturbed by the drift kink instability as shown in Fig. 4b. Finally, the reconnection takes place at $x = 82\,\Delta(= -12\,R_{\mathrm{E}})$ and the plasmoid is formed tailward (see, for example, [6], [47]). Therefore, the magnetic field at $x = -12\,R_{\mathrm{E}}$ is reversed to southward as shown in Fig. 4c and 4d. At the same time, due to the reconnection, the electrons are pushed away from the diffusion region and earthward plasma flows are generated.

Figure 5 shows the evolution of the thinned current sheet with a southward IMF [11], [12]. At 0.10 UT (1216), when the front of the solar wind with the southward IMF has reached $x = 104\,\Delta\,(= -34\,R_{\mathrm{E}})$, the magnetic field is thinned and the current density is intensified near the Earth ($x < 87\,\Delta$) as shown in Fig. 5a (see also Fig. 3b) due to the duskward electric field ($E_y \approx -v_{sol} \times B_{IMF}$). The intensified current density extends deeper into the tail as the southward IMF moves tailward. At 0.20 UT (1280), reconnection takes place at $x = 85\,\Delta(= -15\,R_{\mathrm{E}})$ (see also Fig. 3c). Due to the reconnection and plasmoid (see Fig. 3d) the region of high current density shifts toward the Earth and the distant tail (Fig. 5c). Then the current sheet becomes localized near the Earth as shown in Fig. 5d. It should be noted that the weak B_z field and an anomalous resistivity due to the kinetic (drift kink) instability [54], [55] may excite the tearing instability [21]. Furthermore, simulations show that the sheet current in the near-Earth magnetotail decreases (disrupts), which may be

related to the current disruption that gives rise to the wedge current [54], [55].

Figure 6 shows the electron density in the equatorial plane of the magnetosphere at 0.10 UT (1216) (a), 0.20 UT (1280) (b), 0.30 UT (1344) (c), and 0.40 UT (1408) (d) near the Earth (the maximum electron density is normalized to the same value for all panels). The ion density is very similar to the electron density. Due to the earthward electron flow the electrons are piled up in the near-Earth magnetosphere ($r = -5\,R_\mathrm{E}$). As shown in Fig. 5b, at 0.20 UT (1280), the dawnward current becomes maximum around $x = 75\,\Delta(= -5\,R_\mathrm{E})$, which is consistent with the maximum density gradient around $x = 75\,\Delta$ (near the subsolar line ($y = 47\,\Delta$)) in Fig. 6b. Therefore, the dawnward current is generated by the pressure (density) gradient [56], [57]. At a later time (Fig. 6c) the density gradient becomes smaller, which is consistent with the banished dawnward current (0.30 UT (1344)) in Fig. 5. At the same time, energetic electrons (ions) are injected into the inner magnetosphere through the polar cusps around $(x, y) = (72\,\Delta, 48\,\Delta)$. These particles are accelerated at the magnetopause by the reconnection electric field. The earthward moving ions may be accelerated by the dipolarizing magnetic field in the near-Earth magnetosphere.

To illustrate the particle response to the complicated magnetic structure near the null points at 0.20 UT (1280) [58], the electron fluxes are plotted in the dawn-dusk cross-section at the four different x values in Fig. 7 ($x = -8\,R_\mathrm{E}$ (a), $-10\,R_\mathrm{E}$ (b), $-12\,R_\mathrm{E}$ (c), and $-14\,R_\mathrm{E}$ (d)). The x coordinate of the null points ranges from $-12.4\,R_\mathrm{E}$ to $-19.4\,R_\mathrm{E}$ [58]. As shown in Fig. 7, the x component of electron flux (in color) is variable in sign even though the earthward flux (blue) is more dominant and more intense near the Earth (for further details, see Nishikawa [59]). Moreover, the y, z components of electron fluxes in the plasma sheet (shown by arrows) are also affected by the magnetic field near the null points. In Fig. 7d in the near reconnection region the earthward electron flux (blue) is localized and the dawnward electron flux is disturbed by the magnetic field. The synergistic effects of the remnants from the nonlinear stage of the drift-kink instability and the null points are responsible for this magnetic topology and for the localized earthward fluxes. The tailward flows correspond to the return currents that ensure current closure in the diffusion region (see [59]). A recent statistical study shows that the plasma-sheet flow appears to be strongly 'turbulent' (i.e. the flow is dominated by fluctuations that are

unpredictable) [60]. Such turbulent magnetic fields have also been observed in association with the cross-field current instability in the near-Earth magnetotail [61]. Furthermore, it seems that null points are constantly being created and destroyed, which is consistent with the localized and sporadic nature of the reconnection signatures [52], [58], [62], [63], [64]. This idea is supported by the remote observations of the properties of energetic particles accelerated in the course of short "reconnection pulses" [65]. The detailed temporal and spatial evolution of null points and its relationship with BBFs need to be investigated in the near future.

To investigate the increased particle population in the inner plasma sheet, the particles that lie in the box in the near-Earth magnetotail ($80 \leq x/\Delta \leq 110$, $40 \leq y/\Delta \leq 56$, $40 \leq z/\Delta \leq 56$) are labeled at 0.30 UT (1344) and they are traced back in time to 0.10 UT (1216). (The particle marked in red move to the near-Earth magnetotail marked in black in 20 minutes.) Figure 8 shows the projections of the ions (Fig. 8a, 8c, and 8e) and the electrons (Fig. 8b, 8d, and 8f) on the $x-z$, $x-y$, and $y-z$ planes. (The particles at 0.30 UT (1344) and 0.10 UT (1216) are plotted in black and red, respectively.) As shown in Fig. 8a, 8c, and 8e, ions drift inward from the low-latitude boundary layers and the mantle. As shown in Fig. 8c and 8e, more ions drift into the region from the dawnside, while more electrons drift into the region from the dusk side as shown in Fig. 8d and 8f. Few electrons come from further down the magnetotail (Figs. 8b and 8d). These particle drifts are consistent with the dawn-dusk electric field accompanying the southward IMF.

Figure 9 displays results of a similar particle-traceback from the inner magnetosphere. In order to check the immediate effects of the magnetic reconnection at the magnetopause and in the near-Earth magnetotail, Nishikawa [11] has investigated where particles come from into the inner magnetosphere ($r < 6\,R_{\rm E}$)) at 0.30 UT (1344). As in Fig. 8, Fig. 9 shows the projections of ions (Fig. 9a, 9c, and 9e) and electrons (Fig. 9b, 9d, and 9f) onto the $x-z$, $x-y$, and $y-z$ planes. (The particles at 0.30 UT (1344) and 0.10 UT (1216) are plotted in black and red, respectively.) Most of both the ions and the electrons (marked in red) come from the nearby magnetosphere. However, some ions move in from the dayside (toward dawn) magnetopause as shown in Fig. 9a, 9c, and 9e, while electrons drift from the afternoon-side magnetopause. This tendency is consistent with the drifts

shown in Fig. 8. As shown in Fig. 2, the magnetic reconnection occurring at the dayside magnetopause gives rise to strong and rapid particle entry into the inner magnetosphere. It is clearly necessary to trace particles to investigate the particle dynamics more precisely; truly self-consistent particle dynamics can be studied only by particle simulations.

Northward to dawnward turning IMF

At -1.00 UT (768) [40], [41], [42] a northward IMF ($B_z^{IMF} = 0.2$), (for comparison, the average B at the dayside magnetopause ($\approx 10\,R_{\rm E}$) is nearly 2.8) is switched on, and the northward-IMF front reaches about $x = 120\,\Delta$ at 0.20 UT (1280). The Alfvén velocity with this IMF is $v_A/c = 0.05(\bar{n}_i)^{-1/2} = 0.05$ for the average ion density $\bar{n}_i = 1$. At 0.10 UT (1216) the northward IMF is switched to dawnward at $x = 66\,R_{\rm E}$. In this case the amplitude of the IMF is kept constant and the IMF is rotated counter clockwise (viewed from the Sun) [24].

The magnetic field lines at 1.30 UT (1728) are plotted in Fig. 10, in three dimensions (a), and as projections on the $x - z$ plane (b), on the $y - z$ plane (c), and on the $x - y$ plane (d). The dawnward IMF connects to the north dayside cusp and extends from the south dayside cusp towards the dawnside. Later, more dawnward IMF connects with the magnetospheric field along the flank toward the tail.

In order to check the interaction of the dawnward IMF with the magnetic field near the Earth at 2.00 UT (1920), Fig. 11 shows cross-sectional slices (viewed from the tail, with the duskside on the left) of the magnetic field strength $|\mathbf{B}|$ at three x positions $67\,\Delta(= 3\,R_{\rm E})$ (a), $71\,\Delta(= -1\,R_{\rm E})$ (b), $73\,\Delta(= -3\,R_{\rm E})$ (c), and the electron thermal energy (see Fig. 12d) at $x = 71\,\Delta(= -1\,R_{\rm E})$ (d); (See the accompanying paper with a duskward IMF by White et al. [66]. Due to the opposite viewing point (from the Sun) the results look similar.) The Earth center is at $(y, z) = (47.5\,\Delta,\, 48\,\Delta)$. It should be noted that in Figs. 11a, 11b, and 11c the maximum and minimum values are set in such a way as to highlight the islands of very weak magnetic field. With other diagnostics at different x positions as in Figs. 11a, 11b, and 11c, the simulation results show that distinct regions of very weak magnetic field emanate from the regions of dayside cusps and radiate tailward [24], [66]. The null lines (reconnection grooves) lie in the very weak magnetic field islands as shown in the three

consecutive slices (Figs. 11a, 11b, and 11c). For example, at $x = 73\,\Delta(= -3\,R_{\mathrm{E}})$ as shown in Fig. 11c, the null lines (reconnection grooves) are located at $(y,\,z) = (36\,\Delta,\,42\,\Delta)\,(=$ $(11\,R_{\mathrm{E}},\,-6\,R_{\mathrm{E}}))$ and $= (58\,\Delta,\,57\,\Delta)\,(= (-11\,R_{\mathrm{E}},\,9\,R_{\mathrm{E}}))$. Combining the two plates shown in Figs. 11b and 11d (at $x = 71\,\Delta(= -1\,R_{\mathrm{E}})$), one can see that the reconnection groove (Fig. 11b) is an access region for magnetosheath plasma [24], [66]. It is also a heating region for the plasma (electrons) as shown in Fig. 11d (duskside) indicating a large dawn-dusk asymmetry in the near-Earth magnetosphere [67]. In Fig. 11d, through the groove $((y,\,z) = (37\,\Delta,\,41\,\Delta)(= (10\,R_{\mathrm{E}},\,-7\,R_{\mathrm{E}})))$ magnetosheath plasma (electrons) has accessed the deep regions of the magnetosphere via field lines that go near the magnetopause and is heated [68]. Another figure (not shown here) shows that deep connection between the magnetopause flank weak-field region begins already on the dayside [24], [66]. However, this deep connection is most fully recognized tailward of Earth, where it is best seen in cross-sectional views of the tail as in Fig. 12.

Figure 12 shows a dawn-dusk cross-section of the tail at $x = 85\,\Delta(= -15\,R_{\mathrm{E}})$ viewed from further down the tail at 2.00 UT (1920) [69], [47]. (The subsolar line is located at $(y,\,z) = (47.5\,\Delta,\,48\,\Delta)$.) Contours of B_x are shown in Fig. 12a, which outlines the tail and shows the northern (dark blue) and southern (dark red) lobes. The 'neutral line' is defined by the condition $B_x = 0$. Note that the neutral sheet is well defined across the midplane of the tail, as expected, but that it also extends as a sharply defined feature along the southern dusk flank and less clearly along the northern dawn flank, which confirms the observation presented in [24], [66]. The extended current sheet has a sigmoid shape. This geometrical structure is referred to as the cross-tail S [24], [66]. The flank parts of the cross-tail S lie in the flank, weak-field region which is extended from the dayside magnetopause [24], [66]. Other aspects of the cross-tail S are also seen in the contours of field strength $|\mathbf{B}|$ as shown in Fig. 12b. Note the two islands of very weak field $((y,\,z) = (31\,\Delta,\,35\,\Delta)(= (16\,R_{\mathrm{E}},\,-13\,R_{\mathrm{E}}))$ and $(66\,\Delta,\,64\,\Delta)(= (-18\,R_{\mathrm{E}},\,16\,R_{\mathrm{E}})))$ that seem to mark the point on each flank where the tail part of the cross-tail S joins the magnetopause null lines (see also the islands of very weak magnetic field in Figs. 11a, 11b, and 11c). The thermal energies $(E_{th}^{j} = 0.5 * \Sigma m_j (v^j - v_a^j)^2$, where $v_a^j = \Sigma v^j / \Sigma j$ and $j = i, e)$ of ions (Fig. 12c) and electrons (Fig. 12d) are shown. The region of

elevated ion temperature associated with the flank null lines $((y, z) = (31\,\Delta,\, 35\,\Delta)\,(=\, (16\,R_{\mathrm{E}},\, -13\,R_{\mathrm{E}})$, the dawnside is not so clear) is evidently in geometrical connection with the plasma sheet, revealed here as a cross-tail bar of elevated ion temperature (located between the cold ion lobes (dark blue) as shown in Fig. 12c). The elevated ion temperature domains (around $(y, z) = (30\,\Delta,\, 41\,\Delta)\,(=\, (17\,R_{\mathrm{E}},\, -7\,R_{\mathrm{E}}))$ describe the figure of the cross-tail S (again the dawnside is not so clear). This feature is also seen in the electron temperature; however, the highest temperature is located in the center of plasma sheet $((y, z) = 48\,\Delta,\, 47\,\Delta)\,(=\, (-1R_{\mathrm{E}},\, -1R_{\mathrm{E}}))$ as shown in Fig. 12d.

As expected from the large particle entry (shown in Fig. 11d), electrons are injected into the inner magnetosphere from the duskside magnetopause which is also shown in the equatorial plane at the same time 2.00 UT (1920). Comparing with the previous time 1.30 UT (1728), the electron density is increased by about two times in the near-Earth magnetotail. Furthermore, the inner edge is moved from $79\,\Delta(=\,-9\,R_{\mathrm{E}})$ to $75\,\Delta(=\,-5\,R_{\mathrm{E}})$. The magnetic field in the duskside magnetopause (around $(x, y) = (70\,\Delta,\, 40\,\Delta)\,(=\, (0.5\,R_{\mathrm{E}},\, 7\,R_{\mathrm{E}}))$ becomes disturbed, which corresponds to the reconnection groove. It should be noted that the electron density in the noon-midnight meridian cross-section plane at the same time 2.00 UT (1920) shows no reconnection in the near-Earth magnetotail. This may be explained by the fact that the penetrated IMF B_y component (as shown by the arrows in Figs. 12a and 12b) reduces the growth rate of the tearing instability (above a critical B_y/B_z, the IMF with finite B_y increases the yy component of the electrical conductivity sharply.) [70], [71]. Consequently, no reconnection occurs in the near-Earth magnetotail, so there may be no substorm onsets. However, particle injection takes place through the reconnection groove at the duskside magnetopause, which may be related to pseudo-substorm onsets [68].

IV. Discussion

The results presented here show that even with the modest grid size of 215 by 95 by 95 cells, a three-dimensional fully kinetic model is able to portray the complete magnetosphere with some of the basic characteristics observed for southward and dawnward turning IMFs. For southward IMF, the simulation results show reconnection taking place at the dayside magnetopause and increased particle entry into the magnetosphere. The structure, motion,

and occurrence of magnetic reconnection at the dayside magnetopause have been observed [72], [73]. Phan and Paschmann [72] observed that the normal velocity v_n is nearly constant through the magnetopause (as shown in Fig. 9 in [72]). In the case of southward IMF, since both the $\mathbf{E}$ and the $\mathbf{B}$ fields reverse, $\mathbf{E} \times \mathbf{B}$ will not reverse in the dayside magnetopause which is consistent with the observations. Therefore this reversed $\mathbf{E}$ field through the magnetopause current leads to nonzero $\nabla \times \mathbf{E}$. Investigation of this structure ($\nabla \times \mathbf{E} \neq 0$) and its effects on particle diffusion (due to reconnections) requires further diagnosis, and improved simulations with better resolutions in space and time.

A southward IMF causes magnetic field stretching in the near-Earth plasma sheet. The cross-field current thins and intensifies, which excites a kinetic (drift kink) instability along the dawn-dusk direction. Note that theoretical analysis [15], [16], [74] and particle simulations [17], [18] indicate that the collisionless tearing is stabilized by the electron compressibility which results from the finite normal magnetic component (B_z) in the central plasma sheet. The reduced B_z with a kinetic (drift kink) instability in the central plasma sheet apparently allows the collisionless tearing to grow [21]. More precisely, the plasma transport across tubes caused by the kinetic (drift kink) instability appears to reduce the electron compressibility effect which allows the collisionless tearing instability to grow rapidly. Because of this collisionless tearing instability, magnetic reconnection takes place in the near-Earth magnetotail [52], [58], [75]. At the same time, the nightside magnetic field becomes dipolarized and a plasmoid is formed tailward (see, for example, [6], [47]). A thin, intense current sheet is formed initially and later weakens, as it is observed during substorm breakup and expansion [54], [55].

The 3-D fully kinetic model is also able to produce interesting results with a dawnward IMF. The simulation results show that, due to the dawnward IMF, magnetic reconnection takes place on the flanks of the dayside magnetopause [26], [76], [77]. On each flank, the null line runs tailward from a position near the dayside cusp. A fan of weak field emanates from the region of the dayside cusp and radiates tailward with the null line as its poleward border. This weak-field fan joins onto the plasma sheet and the current sheet to form the cross-tail S that structurally integrates the magnetopause and the tail interior as obtained by both the EMPM [24] and the MHD simulations [66]. This structure might

be a channel of direct entry from the magnetosheath plasma to plasma sheet, in which the entry process heats the magnetosheath plasma to plasma sheet temperatures. At this time step, no reconnection takes place in the near-Earth magnetotail due to the penetrated IMF B_y component (as shown by the arrows in Figs. 12a and 12b) [70], [71]. The new geometrical features confirmed by the 3-D EM particle code (i.e. the weak-field fan on the flank and the cross-tail S) are seen also in maps compiled from IMP 8 data taken at 30 R_{E} down the tail [47], [69].

These initial simulation results with the dawnward IMF suggest that the IMF B_y component is essential for plasma entry [26], [47], [66], [68], [69], [76], [77], [78], [79], [80], [81]. The penetrated IMF B_y component reduces the growth rate of the tearing instability, consequently it delays the occurrence of reconnection in the near-Earth magnetotail. Therefore, it should be noted that the IMF B_y component assists in determining the timing and intensity of substorms as described in the last section. Further simulations will be performed by selecting sets of time-varying solar wind conditions (especially direction). As shown in Fig. 11d, the particle entry through the duskside magnetopause with the IMF B_y component seems to contribute to "theta aurora" [67], [82],

The results reported here suggest that fully three-dimensional electromagnetic particle simulation will become an important tool for the theoretical understanding of Earth's magnetosphere in the not-so-distant future. It is clearly necessary to use more realistic values of m_i/m_e with a larger system and more particles per cell, which relies on the future development of more powerful and faster supercomputers. This would help to establish more precisely the nature of the magnetic reconnection and associated phenomena and to clarify their relation to the observations. At present, however, scaling and grid size remain substantial problems. For example, in the simulations, the Debye length and the thickness of the bow shock are both of the order of an Earth radius, which is of the order of the grid spacing [11], [12], [24]. In the simulations reported here the ion inertial length is resolved, but the electron inertial and Debye lengths are poorly resolved. However, some form of scaling is usually needed in particle simulations, even in one and two dimensions, and yet such simulations are able to reveal some of the physics behind natural phenomena. Further simulations featuring time-dependent IMFs (including B_x, B_y) and plasma clouds

are in progress and will be reported elsewhere.

This EMPM helps us to understand the fundamental physical processes that facilitate particle entry into the inner magnetosphere and ionosphere since particles are traced self-consistently. One of the unique features of this model is that solar-wind particles are injected into the inner magnetosphere through the magnetopause and from the near-Earth magnetotail due to the reconnection and are accelerated self-consistently [11], [12], [24]. Furthermore, the EMPM alone could include these processes well in collisionless regions from the upstream solar wind up to the upper ionosphere without the assistance of other codes. The inclusion of an ionospheric model needs to be developed with much better spatial resolution.

At the present time, the physics of particle entry through the magnetic reconnections with the different IMF directions are being investigated. Further analysis of the evolution of the magnetosphere at this fundamental level will lead to better understanding of substorms (storms) and of the associated particle entry and acceleration, which cause ionospheric disturbances.

In the future, case studies with realistic solar wind conditions obtained by WIND and ACE will be investigated. Post-analysis will be used to identify the scaling law. Due to the smaller mass ratio (at the present time $m_i/m_e = 16$), it is necessary to establish the correlation between the EMPM's results and observations. For example, by comparing accelerated particles injected into the inner magnetosphere with high energy particles observed by MPA instruments on geosynchronous satellites and the Defense Meteorological Satellite Program (DMSP), the model would be verified and its ability to forecast the intensity of substorms and storms could be demonstrated. Already, in the present models, the partial ring current is formed. However, in order to properly account for the ring current during substorms and storms, the simulation parameters need to be adjusted. Particle codes would be able to reveal the self-consistent evolution of ring currents.

In two decades, the MHD simulations have been refined to establish quantitative global modeling [2], [3], [5], [83], [84]. In order to refine the EMPM for quantitative modeling, several major developments have to be made. One of the major necessary developments is to adapt the model for use on more powerful supercomputers such as Cray T3E and

ORIGIN2000 in order to improve spatial and temporal resolutions (with increased mass ratio, i.e., ≈ 100). A code has been developed using High Performance Fortran (HPF) on ORIGIN2000. Consequently, the physics involved in its model will be improved, which will give further verification of the model.

The second important development is to refine the code itself, for instance with a better simulation boundary condition (in the solar wind far from the Earth), and by inclusion of the ionosphere. In order to investigate substorms it is essential to implement the ionosphere which reflects the extreme temporal variability of the magnetosphere and the coupled processes. The present mirror-forced model will be replaced by a simplified ionosphere model where particles injected into the ionosphere are trapped and ionospheric particles are ejected into the magnetosphere. The surface of the model ionosphere will be made conductive to simulate the ionospheric conductivity. This development requires intensive collaboration with ionospheric theorists and experimenters.

As described previously, a new improved EMPM needs to be tested and verified. With a different mass ratio, a new scaling law needs to be found to establish better quantitative modeling based on the observations.

As the global MHD models become an integrated part of many experimental studies, the EMPM will be also involved with these studies. In particular, Cluster II, the Magnetospheric Multiscale Mission, and the Magnetotail Constellation, Dynamics, Reconnection, And Configuration Observatory (DRACO) will provide an excellent opportunity for an integrated study with the EMPM and these advanced observations of macro-, meso, and micro-scale phenomena. This synergetic study will help us to understand unsolved problems such as reconnection, substorm onset and origin of high energy particles injected into the inner magnetosphere. (The color figures can be viewed at http://www.physics.rutgers.edu/ kenichi.)

Acknowledgments

References

[1] J. N. Leboeuf, Tajima, T., Kennel, C. F., and Dawson, J.M., "Global Simulation of the Time-dependent Magnetosphere," *Geophys. Res. Lett.*, 5, 609, 1978.

[2] T. I. Gombosi, D. L. De Zeeuw, C. P. T. Groth, K. G. Powell, A. J. Ridley, and P. Song, "Global MHD modeling of space weather," IEEE Trans, Plasma Sci., this issue, 2000.

[3] C. R. Clauer, T, I. Gombosi, D. I. De Zeeuw A. J. Ridley, K. G. Powell, B. von Leer, Q. F. Stout, and T. E. Holzer, "High performance computing methods applied to predictive space weather," IEEE Trans, Plasma Sci., this issue, 2000.

[4] D. Biskamp, E. Schwartz, and J. F. Drake, "Ion-controlled collisionless magnetic reconnection," *Phys. Rev. Lett., 75*, 3850, 1995.

[5] R. M. Winglee, R. M. Skoug, R. K. Elsen, M. Wilber, R. P. Lin, R. L. Lepping, T. Mukai, S. Kokubun, H. Reme, and T. Sanderson, "IMF induced changes to the nightside magnetotail. A comparison between WIND/Geotail/IMP 8 observations and modeling," *Geophys. Res. Lett., 24*, 947, 1997.

[6] J. Birn, M. Hesse, and K. Schindler, "MHD simulation of magnetotail dynamics," *J. Geophys. Res., 101*, 12,939, 1996.

[7] P. L. Pritchett, F. V. Coroniti and V. K. Decyk, "Three-dimensional stability of thin quasi-neutral current sheets," *J. Geophys. Res., 101*, 27,413, 1996.

[8] C. C. Goodrich, J. G. Lyon, M. Wiltberger, R. E. Lopez, and K. Papadopoulos, "An overview of the impact of the January 10-11, 1997 magnetic cloud on the magnetosphere via global MHD simulation," *Geophys. Res. Lett., 25*, 2537, 1998.

[9] P. L. Pritchett, "Particle-in-cell simulations of magnetosphere electrodynamics," IEEE Trans, Plasma Sci., this issue, 2000.

[10] M. Hesse, "Magnetic reconnection," IEEE Trans, Plasma Sci., this issue, 2000.

[11] K.-I., Nishikawa, "Particle entry into the magnetosphere with a southward IMF as simulated by a 3-D EM particle code," *J. Geophys. Res., 102*, 17,631, 1997.

[12] K.-I. Nishikawa, "Reconnections at near-Earth magnetotail and substorms studied by a 3-D EM particle code," *Global Observations and Models in the ISTP Era*, ed. J. L. Horwitz, W. K. Peterson, and D. L. Gallagher, AGU Geophys. Monograph, *104*, p. 175, 1998.

[13] K. Schindler, "A theory of the substorm mechanism," *J. Geophys. Res., 79*, 2803, 1974.

[14] A. A. Galeev, and L. M. Zelenyi, "Tearing instability in plasma configuration," *Sov. Phys. JETP, Engl. Transl., 43*, 1113, 1976.

[15] B. Lembège, and R. Pellat, "Stability of a thick two-dimensional quasineutral sheet," *Phys. Fluids, 25*, 1995, 1982.

[16] R. Pellat, F. V. Coroniti, and P. L. Pritchett, "Does ion tearing exist?," *Geophys. Res. Lett., 18*, 143, 1991.

[17] P. L. Pritchett, "Effect of electron dynamics on collisionless reconnection in two-dimensional magnetotail equilibria," *J. Geophys. Res., 99*, 5935, 1994.

[18] P. L. Pritchett, and J. Büchner, "Collisionless reconnection with a minimum in the equatorial magnetic field and with magnetic shear," *J. Geophys. Res., 100*, 3601, 1995.

[19] P. L. Pritchett, and F. V. Coroniti," Formation of thin current sheets during plasma sheet convection," *J. Geophys. Res., 100*, 23,551, 1995.

[20] J. Birn, J. F. Drake, M. A. Shay, B. N. Roger, R. E. Denton, M. Hesse, M. Kuznetsova, Z. W. Ma, A. Bhattacharjee, A. Otto, and P. L. Pritchett, "GEM magnetic reconnection challenge," *J. Geophys. Res.*, accepted, 1999b.

[21] P. L. Pritchett, and F. V. Coroniti, "The role of the drift kink modes in destabilizing thin current sheets," *J. Geomagn. Geoelectr., 48*, 833, 1996.

[22] P. L. Pritchett, F. V. Coroniti and R. Pellat, "Convection-driven reconnection and the stability of the near-Earth plasma sheet," *Geophys. Res. Lett., 24*, 873, 1997.

[23] P. L. Pritchett, and F. V. Coroniti, "Interchange and kink modes in the near-Earth plasma sheet and their associates plasma flows," *Geophys. Res. Lett., 24*, 2925, 1997.

[24] K.-I. Nishikawa, "Particle entry through reconnection grooves in the magnetopause with a dawnward IMF as simulated by a 3-D EM particle code," *Geophys. Res. Lett., 25*, 1609, 1998.

[25] G. Rostoker, "Phenomenology and physics of magnetospheric substorms," *J. Geophys. Res., 101*, 12,955, 1996.

[26] D. N. Baker, T. I. Pulkkinen, V. Angelopoulos, W. Baumjohann, and R. L. McPherron, "Neutral line model of substorms: Past results and present view," *J. Geophys. Res., 101*, 12,975, 1996.

[27] V. A. Sergeev, T. I. Pulkkinen, and R. J. Pellinen, "Coupled-mode scenario for the magnetospheric dynamics," *J. Geophys. Res., 101*, 13,047, 1996.

[28] W. Daughton, "Kinetic theory of the drift kink instability in a current sheet," *J. Geophys. Res., 103*, 29,429, 1998.

[29] W. Daughton, "The unstable eigenmodes of a neutral sheet," *Phys. Plasmas 6*, 1329, 1999.

[30] O. Buneman, C. W. Barnes, J. C. Green, and D. E. Nielsen, "Review: Principles and capabilities of 3-D, E-M particle simulations," *J. Comput. Phys., 38*, 1, 1980.

[31] O. Buneman, "TRISTAN: The 3-D, E-M particle code," in *Computer Space Plasma Physics, Simulation Techniques and Software*, edited by H. Matsumoto and Y. Omura, p. 67, Terra Sci., Tokyo, 1993.

[32] J. Villasenor, and O. Buneman, "Rigorous charge conservation for local electromagnetic field solvers," *Comp. Phys. Commun., 69*, 306, 1992.

[33] E. L. Lindman, "Free-space boundary conditions for the time dependent wave equation," *J. Comp. Phys., 18*, 66, 1975.

[34] T. Neubert, R. H. Miller, O. Buneman, and K.-I. Nishikawa, "The dynamics of low-β plasma clouds as simulated by a 3-dimensional, electromagnetic particle code," *J. Geophys. Res., 97*, 12,057, 1992.

[35] K.-I. Nishikawa, O. Buneman, and T. Neubert, "New aspects of whistler waves driven by an electron beam studied by a 3-D electromagnetic code," *Geophys. Res. Lett., 21*, 1019, 1994.

[36] J. Zhao, J.I. Sakai, K.-I. Nishikawa, and T. Neubert, "Relativistic particle acceleration in an electron-positron plasma with a relativistic electron beam," *Phys. Plasmas, 1*, 4114, 1994.

[37] K.-I. Nishikawa, J.-I. Sakai, J. Zhao, T. Neubert, and O. Buneman, "Coalescence of two current loops with kink instability simulated by 3-D EM particle code," *Astrophys. J., 434*, 363, 1994.

[38] J. Zhao, J. I. Sakai, and K.-I. Nishikawa, "Particle simulation on collision between a plasma cloud and a current loop," *Astrophys. J. Lett., 449*, L-161, 1995.

[39] J. Zhao, J. I. Sakai, and K.-I. Nishikawa, "Coalescence of two parallel current loops in a non-relativistic electron-positron plasma," *Phys. Plasmas, 3*, 844, 1996.

[40] O. Buneman, T. Neubert, and K.-I. Nishikawa, "Solar wind-magnetosphere interaction as simulated by a 3D, EM particle code," *IEEE Trans. Plasma Sci., 20*, 810, 1992.

[41] O. Buneman, K.-I. Nishikawa, and T. Neubert, "Solar wind-magnetosphere interaction as simulated by a 3D EM particle code," *Space Plasmas: Coupling Between Small and Medium Scale Processes*, Geophys. Monogr. Ser., vol. 86, edited by M. Ashour-Abdalla, T. Chang, and P. Dusenbery, p. 347, AGU, Washington, D.C., 1995.

[42] K. I. Nishikawa, O. Buneman, and T. Neubert, "Solar wind-magnetosphere interaction as simulated by a 3-D EM particle code," *Astrophys. Space Sci., 227*, 265, 1995, also in *Plasma Astrophysics and Cosmology*, edited by A. T. Peratt, p. 265, Kluwer Academic Pub., 1995.

[43] S. Y. Fu, Z. Y. Pu, Z. X. Liu, and Q. G. Zong, "Simulation study on stochastic reconnection at the magnetopause," *J. Geophys. Res., 100*, 12,001, 1995.

[44] D. W. Swift, "Use of a hybrid code for global-scale plasma simulation," *J. Comput. Phys., 126*, 109, 1996.

[45] N. Omidi, H. Karimabadi, and D. Krauss-Varban, "Hybrid simulation of the curved dayside magnetopause during southward IMF," *Geophys. Res. Lett., 25*, 3273, 1998.

[46] D. Krauss-Varban, H. Karimabadi, and N. Omidi, "Two-dimensional structure of the coplanar and non-coplanar magnetopause during reconnection," *Geophys. Res. Lett., 26*, 1235, 1999.

[47] R. J. Walker, and T. Ogino, "A global magnetohydrodynamic simulation of the origin and evolution of magnetic flux ropes in the Magnetotail," *J. Geomagn. Geoelectr., 48*, 765, 1996.

[48] J. R. Kan, "A globally integrated substorm model: Tail reconnection and magnetosphere-ionosphere coupling," *J. Geophys. Res., 103*, 11,787, 1998.

[49] S. Ohtani, F. Creutzberg, T. Mukai, H. Singer, A. T. Y. Lui, M. Nakamura, P. Prikyl, K. Yumoto, and G. Rostoker, "Substorm onset timing: The December 31, 1995, event," *J. Geophys. Res., 104*, 22,713, 1999.

[50] K.-I. Nishikawa, and S. Ohtani, "Evolution of thin current sheet with a southward IMF studied by a 3-D EM particle code," *J. Geophys. Res., 105*, 13,017, 2000.

[51] Z. Zhu, and R. M. Winglee, "Tearing instability, flux ropes, and the kinetic current sheet kink instability in the Earth's magnetotail: A three-dimensional perspective from particle simulations," *J. Geophys. Res., 101*, 4885, 1996.

[52] J. Büchner, "Three-dimensional magnetic reconnection in astrophysical plasmas - Kinetic approach," *Astrophysics and Space Sciences, 264*, 25, 1999. 1999.

[53] L. R. Lyons, "Substorms: Fundamental observational features, distinction from other disturbances, and external triggering," *J. Geophys. Res., 101*, 13,011, 1996.

[54] A. T. Y. Lui, "A synthesis of magnetospheric substorm models," *J. Geophys. Res., 96*, 1849, 1991.

[55] A. T. Y. Lui, "Current disruption in the Earth's magnetosphere: Observations and models," *J. Geophys. Res., 101*, 13,067, 1996.

[56] G. K. Park, *Physics of Space Plasmas: An Introduction*, Addison-Wesley, Redwood City, 1991.

[57] J. Birn, M. Hesse, G. Haerendel, W. Baumjohann, and K. Shiokawa, "Flow braking and the substorm current wedge," *J. Geophys. Res., 104*, 19,905, 1999.

[58] D.-S. Cai, and K.-I. Nishikawa, "Topological magnetic structure related to reconnection in the near-Earth

magnetotail with southward IMF studied by three-dimensional electromagnetic particle code," *Geophys. Res. Lett.*, submitted, 1999.

[59] K.-I. Nishikawa, "Global particle simulation study of substorm onset and particle acceleration," *Space Sci. Rev.*, accepted, 2000.

[60] J. E. Borovsky, R. C. Elpic, H. O. Funsten, and M. F. Thomsen, "The Earth's plasma sheet as a laboratory for flow turbulence in high-β MHD," *J. Plasma Phys., 57*, 1, 1997.

[61] A. T. Y. Lui, R. E. Lopez, S. M. Krimigis, R. W. McEntire, L. J. Zanetti, and T. A. Potemra, "A case study of magnetotail current sheet disruption and diversion," *Geophys. Res. Lett, 15*, 721, 1988.

[62] T. Chang, "Sporadic localized reconnections and multiscale intermittent turbulence in the magnetotail, in *Geospace Mass and Energy Flow," Geophys. Monogr. Ser.*, vol. 104, edited by J. L. Horwitz, W. K. Peterson, and D. L. Gallagher, p. 193, AGU, Washington D.C., 1998.

[63] T. Chang, "The role of Coarse-grained helicity and self-organized criticality in magnetotail dynamics," in *Magnetic Helicity in Space and Laboratory Plasmas, Geophys. Monogr. Ser.*, vol. 111, edited by M. R. Brown, R. C. Canfield, and A. A. Pevtson, p. 277, AGU, Washington D.C., 1999.

[64] T. Chang, "Self-organized criticality, multi-fractal spectra, sporadic localized reconnections and intermittent turbulence in the magnetotail," *Phys. Plasmas, 6*, 4137, 1999.

[65] L. M. Zelenyi, A. Taktakishvili, V. N. Lutsenko, and K. Kudela, "Interball observations of the energetic particle spectra in the plasma sheet: Indirect evidence of the multiple explosive-like spontaneous reconnection," in *Substorms-4*, edited by S. Kokubun and Y. Kamide, Kluwer Academic Pub, Dordrecht, p. 521, 1998.

[66] W. White, G. L. Siscoe, G. M. Erickson, Z. Kaymaz, N. C. Maynard, K. D. Siebert, B. U. O. Sonnerup, and D. R. Weimer, "The magnetospheric sash and the cross-tail S," *Geophys. Res. Lett., 25*, 1605, 1998.

[67] J. A. Cumnock, J. R. Sharber, R. A. Heelis, M. R. Hairston, and J. D. Craven, "Evolution of the global aurora during positive IMF B_z and varying IMF B_y conditions," *J. Geophys. Res., 102*, 17,489. 1997.

[68] S. Ohtani, T. A. Potemra, P. T. Newell, L. J. Zanetti, T. Iijima, M. Watanabe, L. G. Blomberg, R. D. Elphinstone, J. S. Murphree, M. Yamauchi, and J. G. Woch, "Four large-scale field-aligned current systems in the dayside high-latitude region," *J. Geophys. Res., 100*, 137, 1995.

[69] Z. Kaymaz, G. Siscoe, J. G. Luhmann, J. A. Fedder and J. G. Lyon, "Interplanetary magnetic field control of magnetotail field: IMP 8 data and MHD model compared," *J. Geophys. Res., 100*, 17,163, 1995.

[70] J. W. Hernandez, W. Horton, and T. Tajima, "Low-frequency mobility response functions for the central plasma sheet with application to tearing modes," *J. Geophys. Res., 98*, 5893, 1993.

[71] Y. Ono, M. Yamada, T. Akao, T. Tajima, and R. Matsumoto, "Ion acceleration and direct ion heating in three-component magnetic reconnection," *Phys. Rev. Lett., 76*, 3328, 1996.

[72] T. D. Phan, and G. Paschmann, "Low-latitude dayside magnetopause and boundary layer for high magnetic shear, 1, Structure and motion," *J. Geophys. Res., 101*, 7801, 1996.

[73] T. D. Phan, G. Paschmann, and B. U. Ö. Sonnerup, "Low-latitude dayside magnetopause and boundary layer for high magnetic shear, 2, Occurrence of magnetic reconnection," *J. Geophys. Res., 101*, 7817, 1996.

[74] G. R. Brittnacher, K. B. Quest, and H. Karimabadi, "On the energy principle and ion tearing in the magnetotail," *Geophys. Res. Lett., 21*, 1591, 1994.

[75] C. E. Parnell, J. M. Smith. T. Neukirch, and E. R. Priest, "The structure of three-dimensional magnetic neutral points," *Phys. Plasmas, 3*, 759, 1996.

[76] M. Fujimoto, A. Nishida, T. Mukai, Y. Saito, T. Yamamoto, and S. Kokubun, "Plasma entry from the flanks

of the near-Earth magnetotail: GEOTAIL observations in the dawnside LLBL and the plasma sheet," *J. Geomag. Geoelectr, 48*, 711, 1996.

[77] M. Fujimoto, T. Mukai, A. Matsuoka, A. Nishida, T. Terasawa, K. Seki, H. Hayakawa, T. Yamamoto, S. Kokubun, and R. P. Lepping, "Dayside reconnected field lines in the south-dusk near-tail flank during an IMF $B_y > 0$ dominated period," *Geophys. Res. Lett., 24*, 931, 1997.

[78] S. W. H. Cowley, J. P. Morell, and M. Lockwood, "Dependence of convective flows and particle precipitation in the high-latitude dayside ionosphere on the X and Y components of the interplanetary magnetic field," *J. Geophys. Res., 96*, 5557, 1991.

[79] J. A. Fedder, S. P. Slinker, J. G. Lyon, and R. D. Elphinstone, "Global numerical simulation of the growth phase and the expansion onset for a substorm observed by Viking," *J. Geophys. Res., 100*, 19.083, 1995.

[80] K. K. Khurana, R. J. Walker, and T. Ogino, "Magnetospheric convection in the presence of interplanetary magnetic field B_y: A conceptual model and simulations," *J. Geophys. Res., 101*, 4907, 1996.

[81] A. Nishida, T. Mukai, T. Yamamoto, Y. Saito, and S. Kokubun, "Magnetotail convection in geomagnetically active times 2. Dawn-dusk motion in the plasma sheet," *J. Geomag. Geoelectr, 48*, 503, 1996.

[82] S.-W. Chang, J. D. Scudder, J. B. Sigwarth, L. A. Frank, N. C. Maynard, W. J. Burke, W. K. Peterson, E. G. Shelley, R. Friedel, J. B. Blake, R. A. Greenwald, R. P. Lepping, G. J. Sofko, J.-P. Villain, and M. Lester, "A comparison of a model for the theta aurora with observations from Polar, Wind, and SuperDARN," *J. Geophys. Res., 103*, 17,367, 1998.

[83] J. A. Fedder, S. P. Slinker, and J. G. Lyon, "A comparison of global numerical simulation results to data for the January 27-28, 1992," Geospace Environment Model challenge, *J. Geophys. Res., 103*, 14,799, 1998.

[84] J. Raeder, J. Berchem, M. Ashour-Abdalla, L. A. Frank, W. R. Paterson, K. L. Acherson, S. Kokubun, T. Yamamoto, and J. A. Slavin, "Boundary layer formation in the magnetotail: Geotail observations and comparisons with a global MHD simulation," *Geophys. Res. Lett., 24*, 951, 1997.
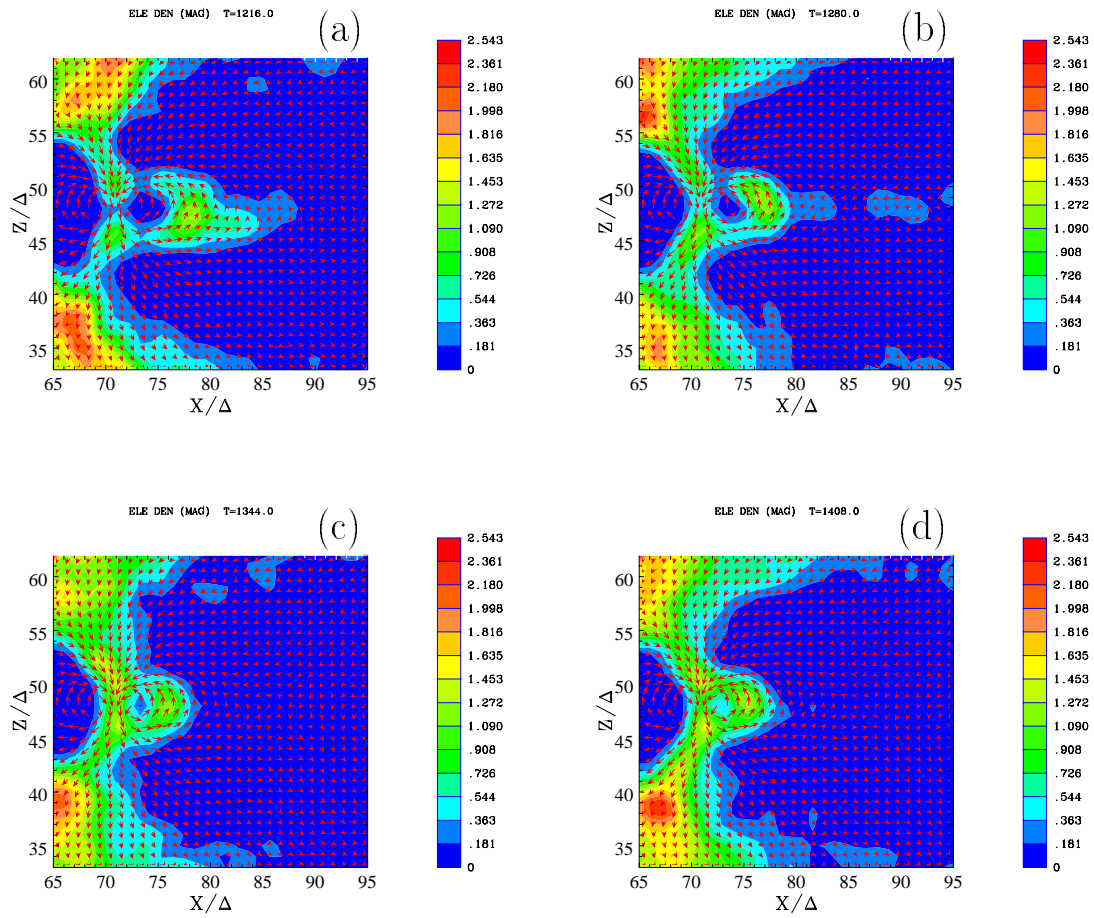
Fig. 1.   Electron density in the noon-midnight meridian $(x - z)$ plane containing the Earth at 0.10 UT (1216) (a), 0.20 UT (1280) (b), 0.30 UT (1344) (c), and 0.40 UT (1408) (d). "Relative amplitude" on the color bar signifies simulation units. The arrows show the magnetic field.
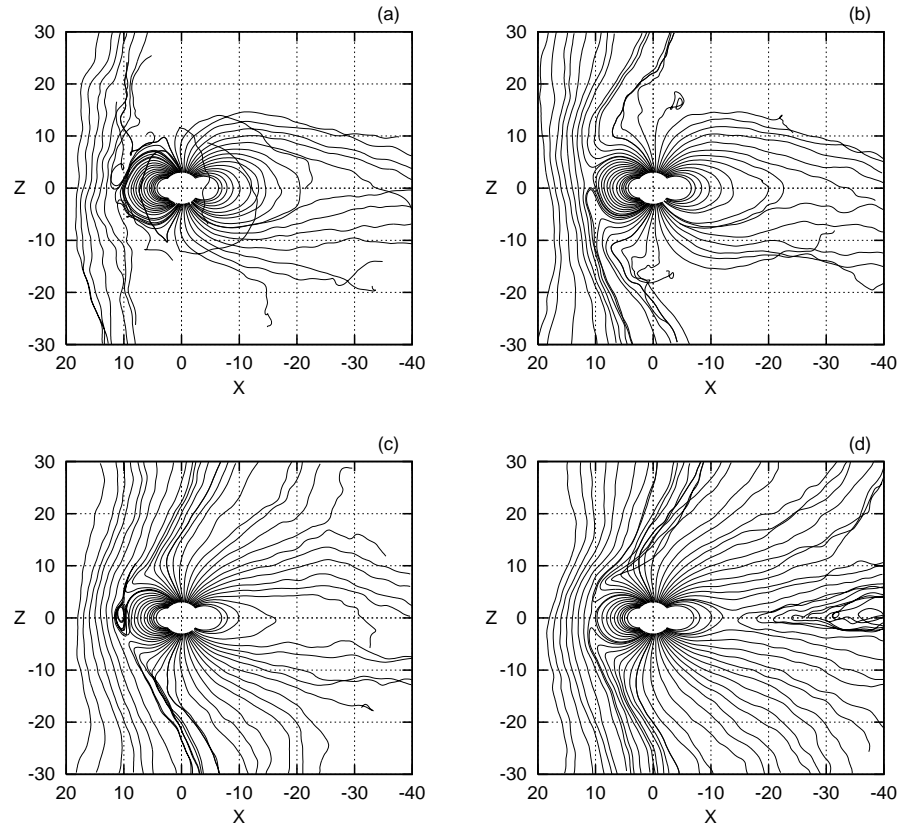
Fig. 2. Magnetic field lines in the noon-midnight meridian $(x - z)$ plane containing the Earth's dipole center at -0.20 UT (1024) (a), -0.10 UT (1088) (b), 0.10 UT (1216) (c), and 0.20 UT (1280) (d). The magnetic field lines are traced from near the Earth $(r = 3\,\Delta\,(\approx 3\,R_E))$ and the subsolar line in the dayside and the magnetotail. Some magnetic field lines are moved dawnward or duskward. The tracing was terminated after a preset number of tracing points or at a preset minimum strength of the total magnetic field (Fig. 1 in [11]).
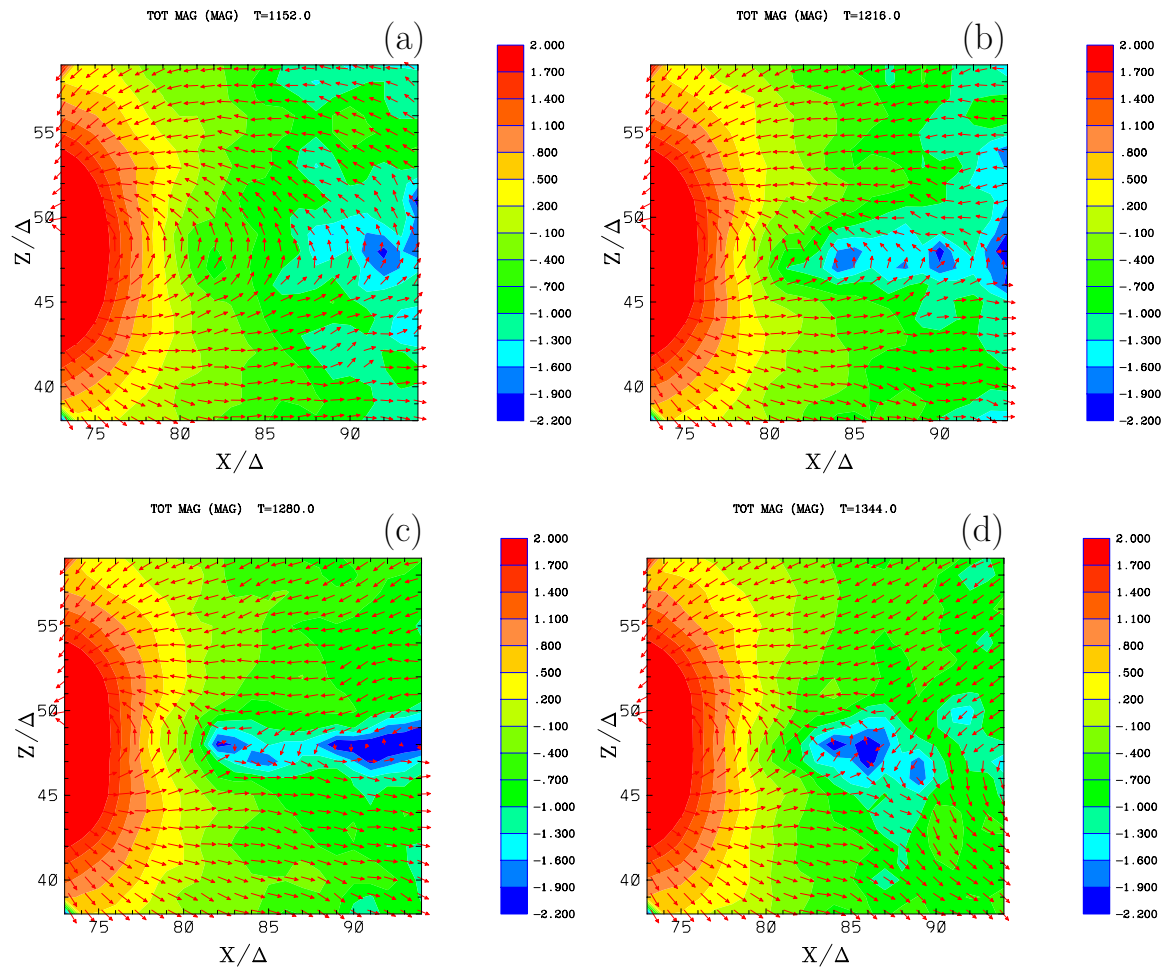
Fig. 3.   The stretching and dipolarization are seen in the total magnetic field strength in the noon-midnight meridian $(x - z)$ plane in the near-Earth magnetotail at 0.00 UT (1152) (a), 0.10 UT (1216) (b), 0.20 UT (1280) (c), and 0.30 UT (1344) (d). The arrows show the magnetic field (Fig. 5 in [50]).
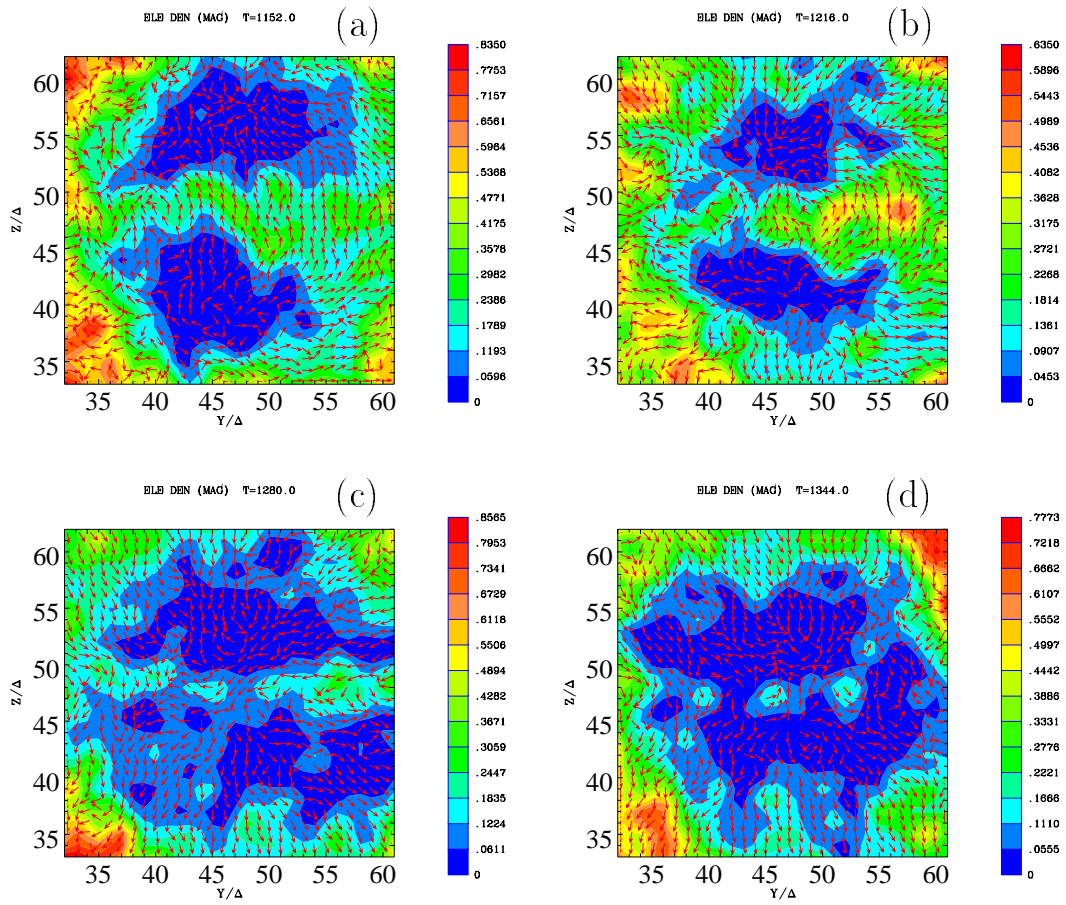
Fig. 4. Electron density in the dawn-dusk $(y - z)$ plane (viewed from th tail) at $x = -15\,R_{\mathrm{E}}$ with the magnetic field shown by arrows at 0.00 UT (1152) (a), 0.10 UT (1216) (b), 0.20 UT (1280) (c), and 0.30 UT (1344) (d). The kinked plasma sheet shows the growth of the kinetic (drift kink) instability, which leads to the tearing instability (Plate 1 in [12]).
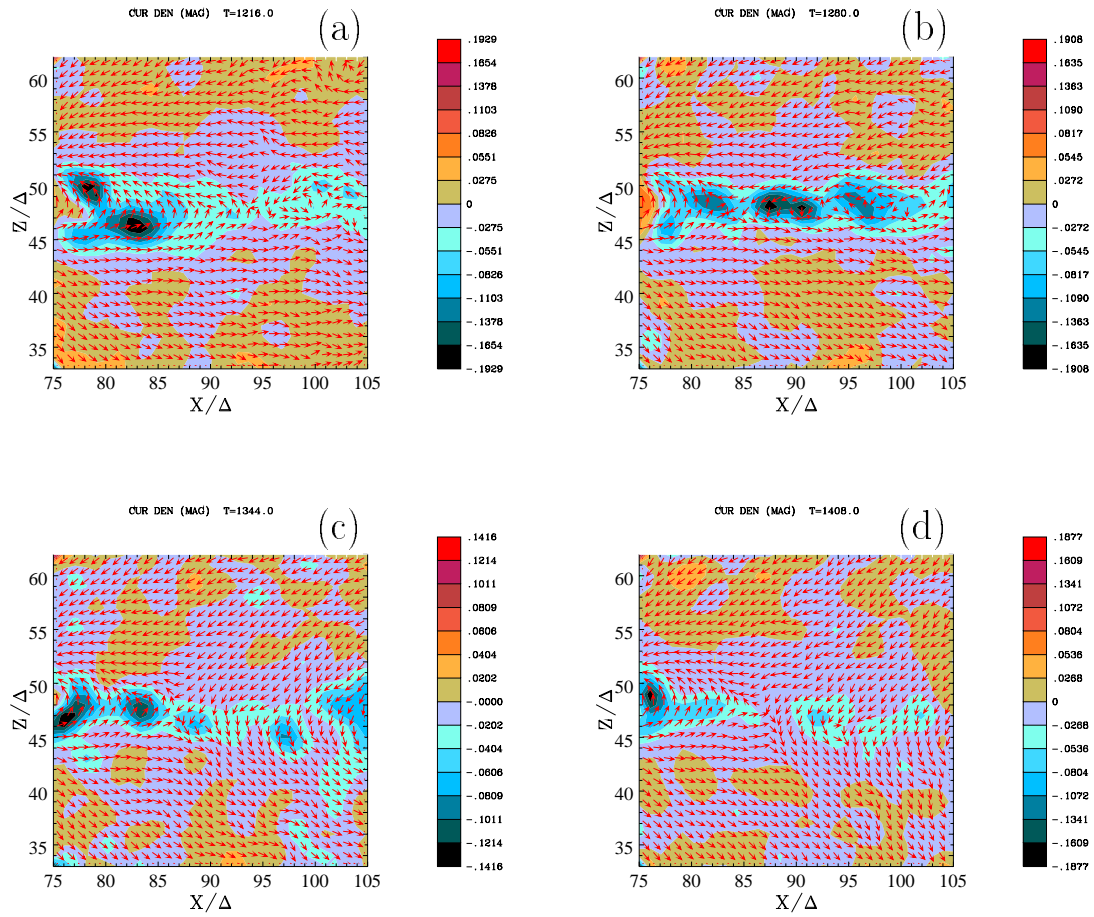
Fig. 5. Thinning sheet current is seen in the current density (J_y) in the noon-midnight meridian $(x-z)$ plane at 0.10 UT (1216) (a), 0.20 UT (1280) (b), 0.30 UT (1344) (c), and 0.40 UT (1408). The arrows show the magnetic field (Fig. 1 in [50]).
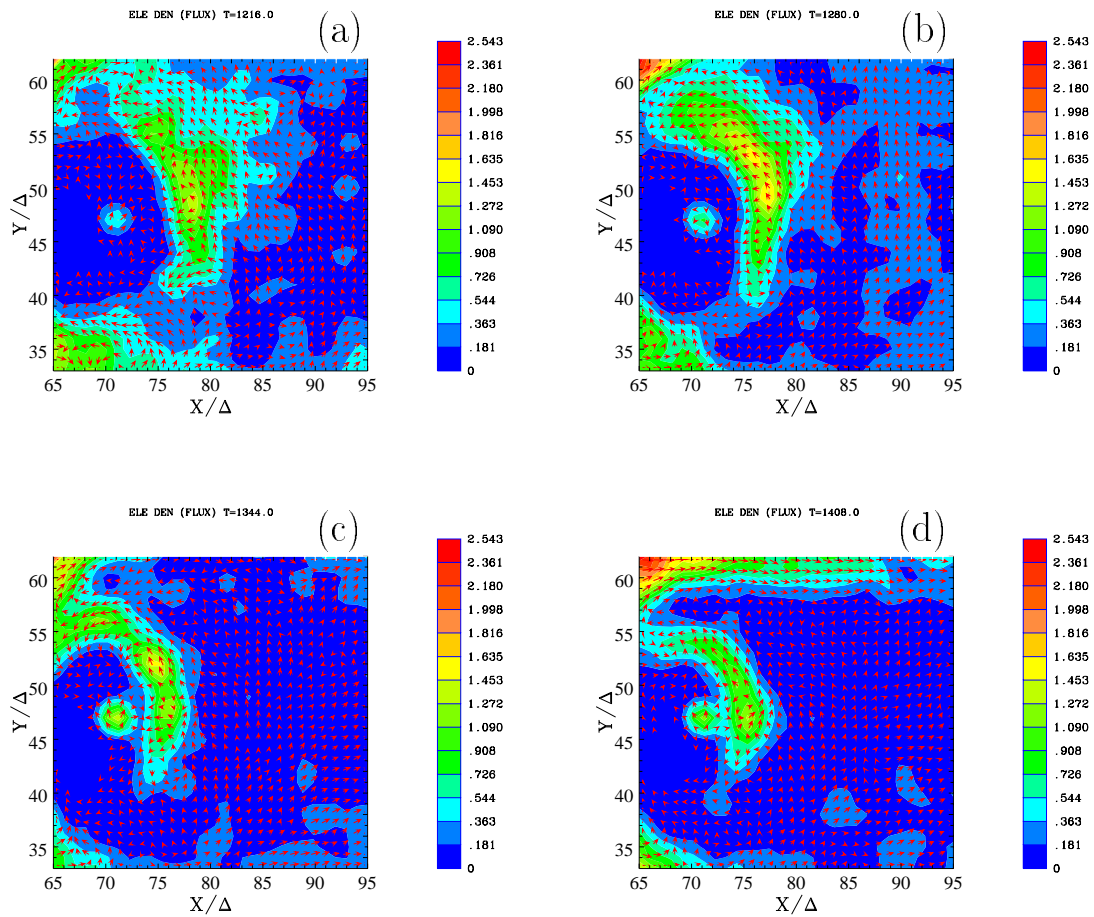
Fig. 6.   Injection of electrons (ions) into the near Earth caused by the reconnection as shown in the equatorial plane at 0.10 UT (1216) (a), 0.20 UT (1280) (b), 0.30 UT (1344) (c), and 0.40 UT (1408) (d). The electrons are also convected toward the Earth where they pile up. The arrows show the electron flux (Fig. 4 in [50]).
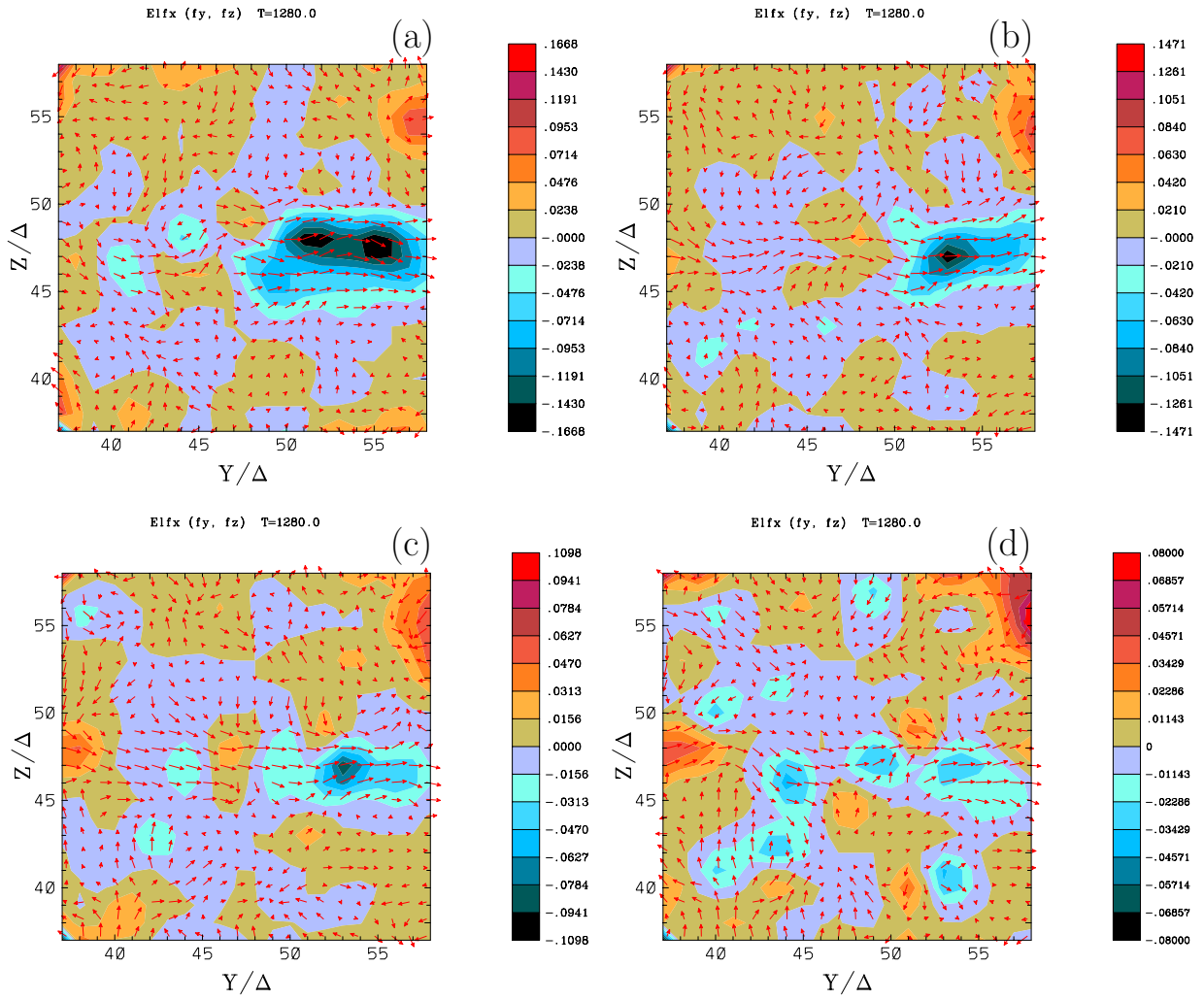
Fig. 7. Dawn-dusk cross-sectional slices at 0.20 UT (1280) show the complex electron-flux structure including the return current that provides current closure in the diffusion region (color: x component, arrows: y, z components) due to the instability and reconnection, at $x =$ (a) $78(\approx -8\,R_E)$, (b) $80(\approx -10\,R_E)$, (c) $82(\approx -12\,R_E)$, and (d) $84(\approx -14\,R_E)$. The substorm line is located at $y = 47, z = 48$.
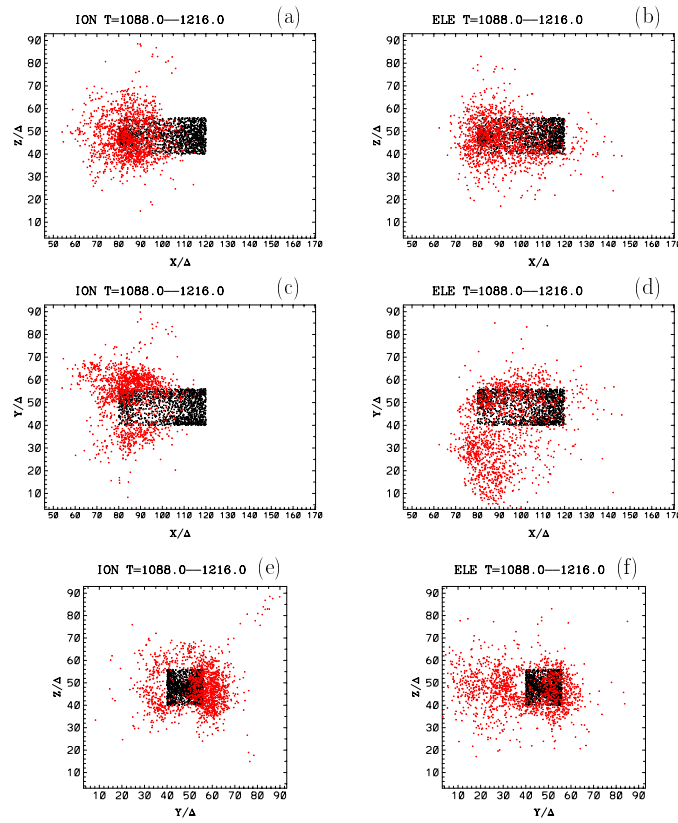
Fig. 8. Here the particle dynamics is checked by tracing. Projections of ions (a, c, and e) and electrons (b, d, and f) are plotted at 0.10 UT (1216) (red) and 0.30 UT (1344) (black) (particles in the box-shaped region in the near-Earth magnetotail ($80 \leq x/\Delta \leq 110$, $40 \leq y/\Delta \leq 56$, $40 \leq z/\Delta \leq 56$)) on the $x - z$ (a and b), $x - y$ (c and d), and $y - z$ planes (e and f) (Plate 5 in [11]).
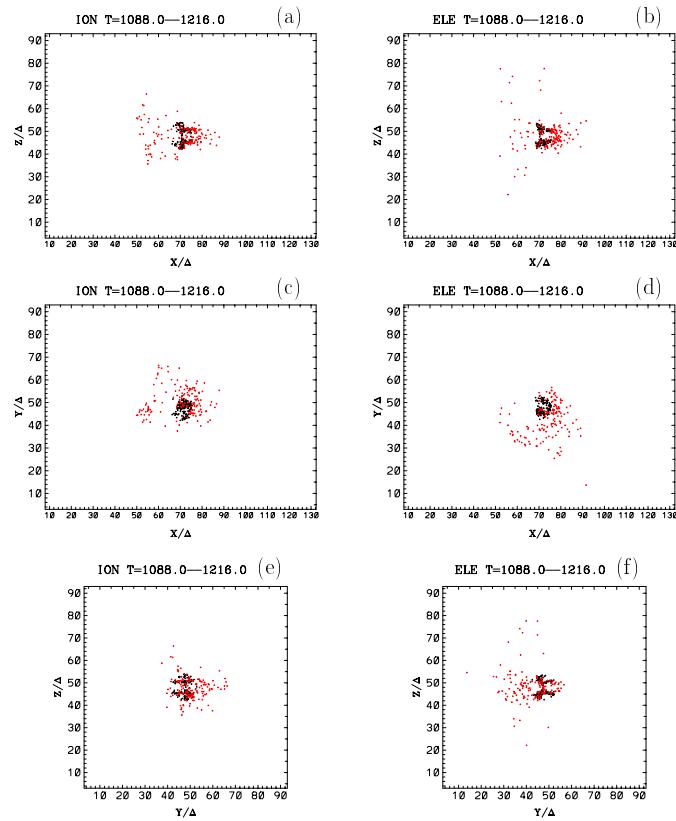
Fig. 9. Again the particle dynamics is checked by tracing. Projections of ions (a, c, and e) and electrons (b, d, and f) are plotted at 0.10 UT (1216) (red) and 0.30 UT (1344) (black) (particles in a spherical region near the Earth $((x - 70.5)^2 + (y - 47.5)^2 + (z - 48)^2 \leq 36)$ on the $x - z$ (a and b), $x - y$ (c and d), and $y - z$ planes (e and f) (Plate 6 in [11]).
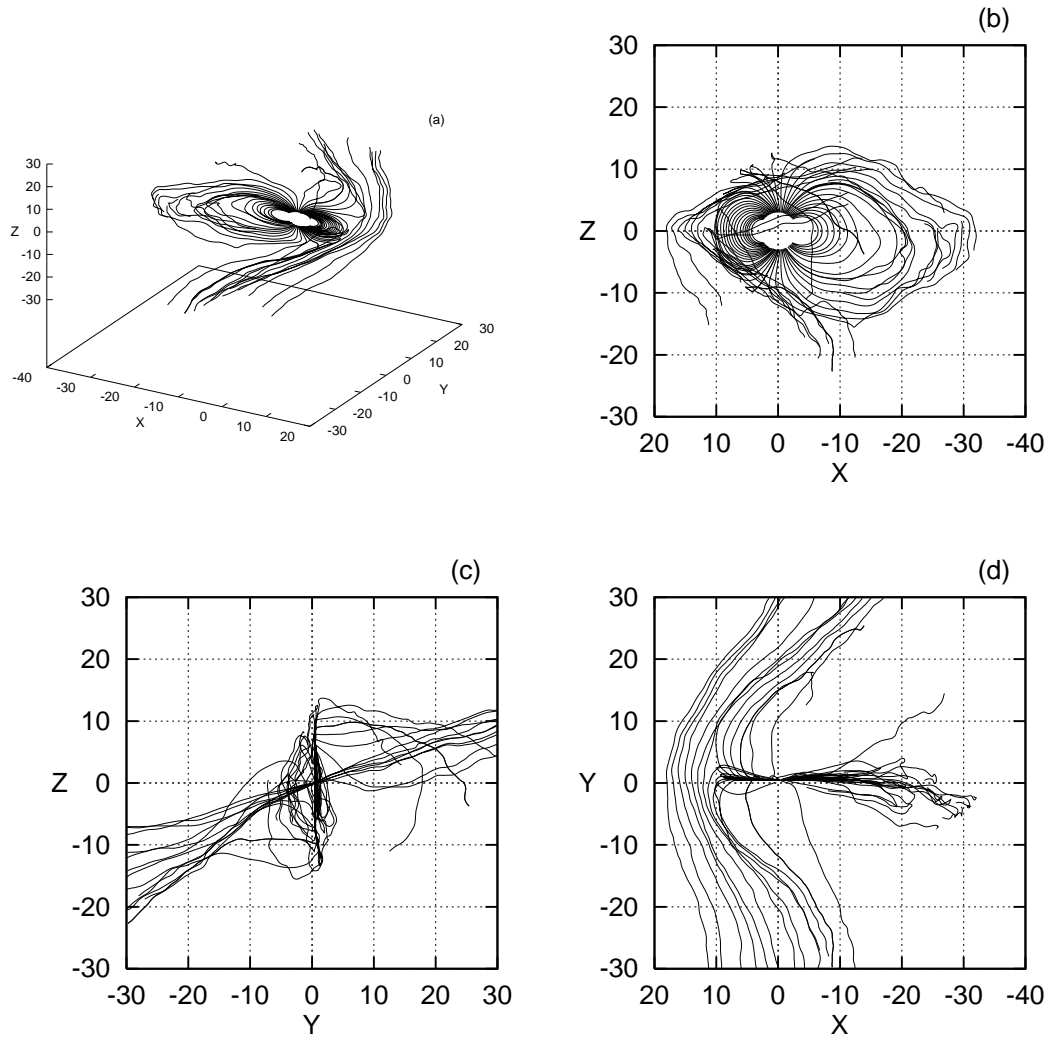
Fig. 10.   The magnetic field lines at 1.30 UT (1728) are shown in three dimensions viewed from the dawnside (a), and in projections onto the $x - z$ plane (b), onto the $y - z$ plane (c), and onto the $x - y$ plane (d) (Fig. 1 in [24]).
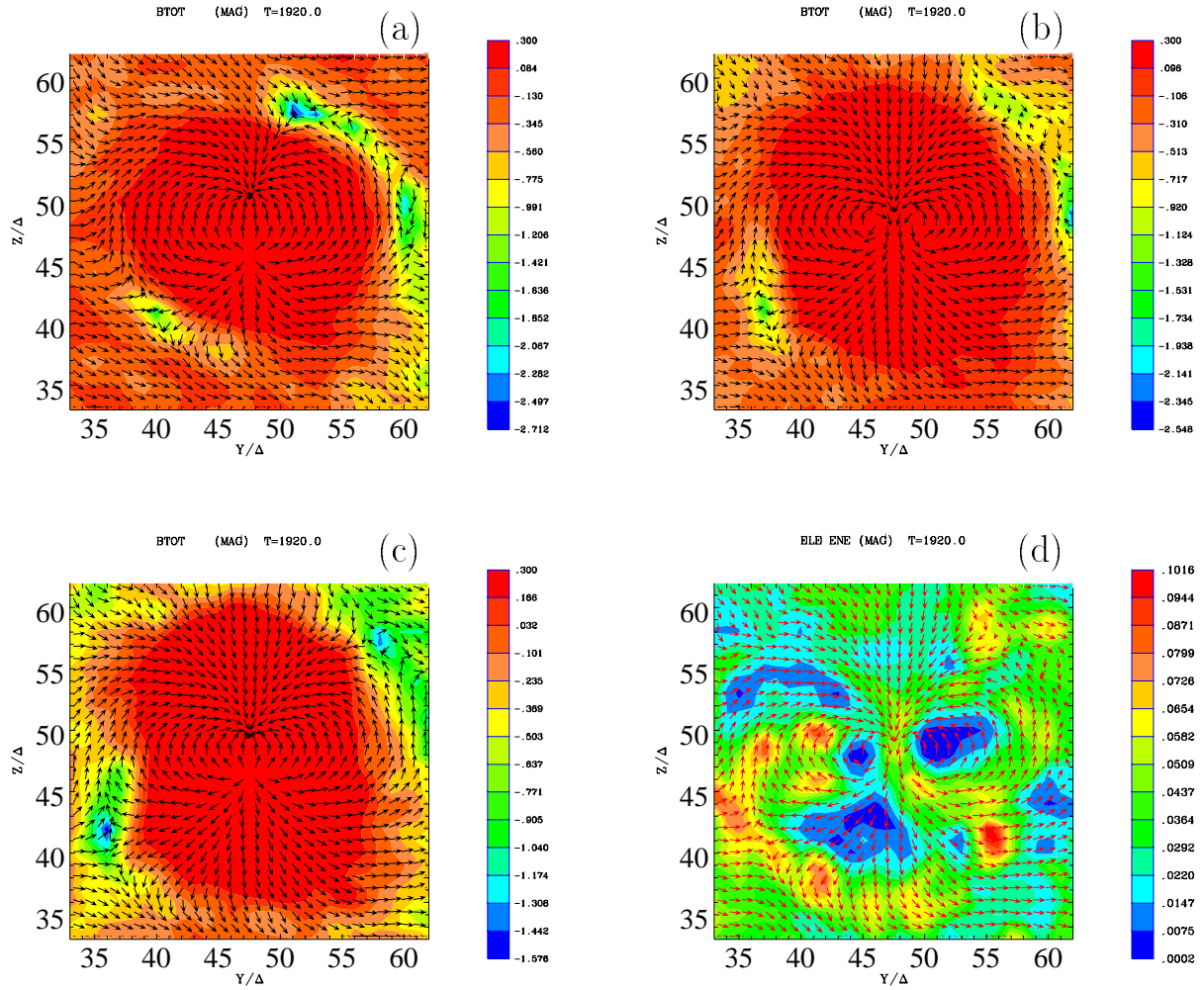
Fig. 11. Dawn-dusk cross-sectional slices of the the total magnetic field $|\mathbf{B}|$ at three x positions (a) $67\,\Delta(\approx 3\,R_E)$, (b) $71\,\Delta(\approx -1R_E)$, (c) $73\,\Delta(\approx -3\,R_E)$, and (d) the electron thermal energy at $x = 71\,\Delta(\approx -1R_E)$ at 2.00 UT (1920) (viewed from the tail). The arrows show the magnetic field, the strength of which has been scaled so as to make the direction clearer for weak fields. Therefore the length of the vectors is not a true representation of the field strength (Fig. 2 in [24]).
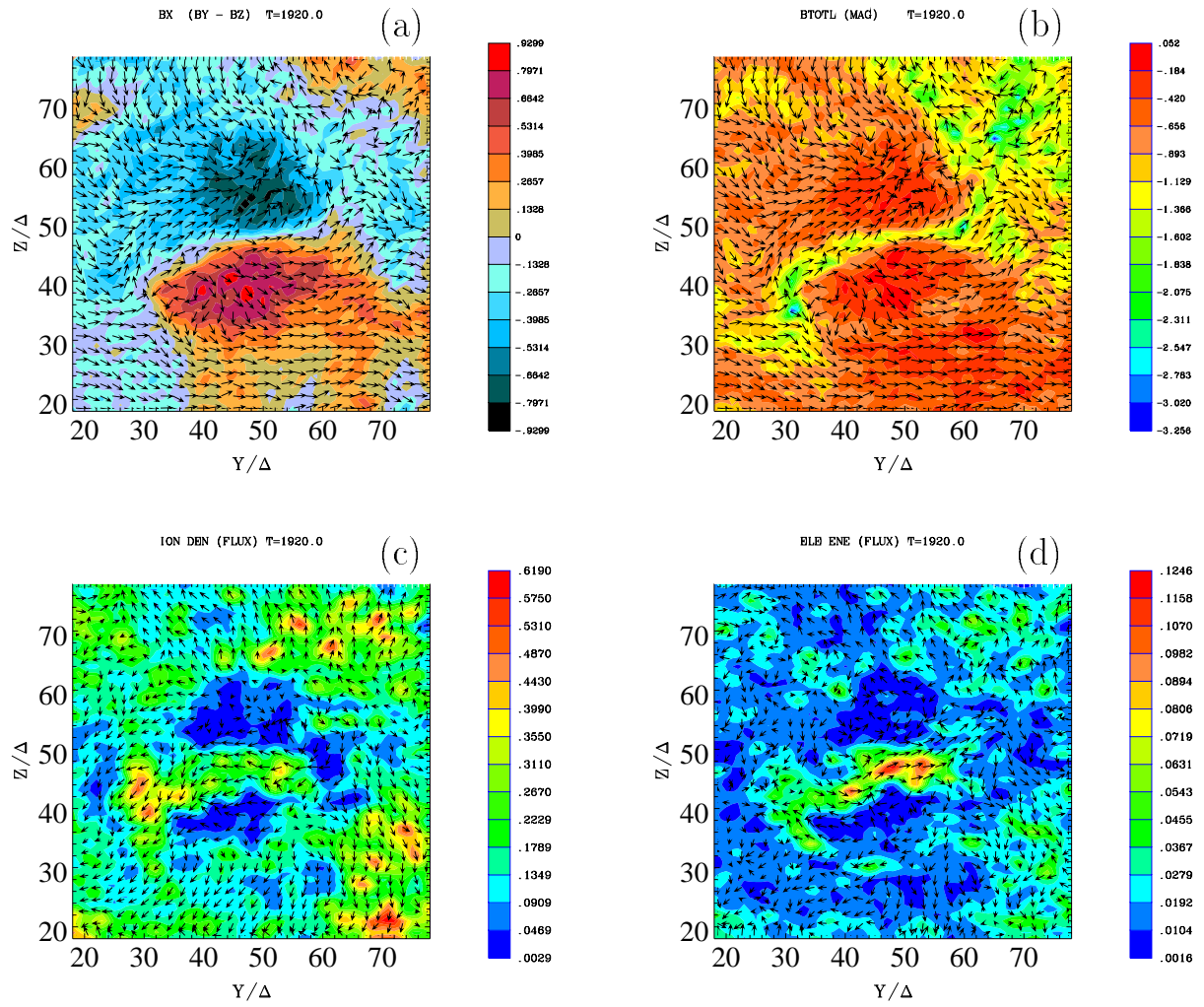
Fig. 12.   Dawn-dusk cross-section of the tail at $x = 85\,\Delta(= -15\,R_E)$ is shown at 2.00 UT (1920); (a) B_x with the magnetic field, (b) the total magnetic field ($|\mathbf{B}|$) with the magnetic field, (c) the ion thermal energy with ion average velocity, and (d) the electron thermal energy with electron average velocity (viewed from the tail). All arrows are scaled (Fig. 2 in [24]).
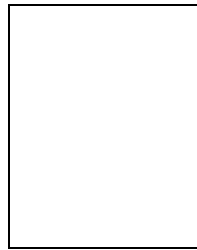
Ken-Ichi Nishikawa was born in Shiga-ken, Japan on April 27, 1949. He received the B.S., M. S., and Ph.D degrees in theoretical plasma physics from Nagoya University, Nagoya, Japan in 1973, 1975, and 1981, respectively. After completing his Ph.D degree, he studied particle simulations with space plasma physics applications with Hideo Okuda at Princeton Plasma Physics Laboratory for two years. In 1984 he joined the Department of Physics and Astronomy, the University of Iowa, as Assistant Research Scientist and he became Associate Research Scientist in 1990. He moved to the Department of Space Physics and Astronomy, Rice University as Research Scientist in 1995. At Rice he developed global simulations with a southward IMF which were included in this review. He studied relativistic jets using a 3-D Relativistic MHD code at the Department of Physics and Astronomy, Louisiana State University for two and a half years. He joined the Department of Physics and Astronomy, Rutgers University as Research Assistant Professor in March 1999. Currently he is investigating substorm and storm triggering mechanisms using 3-D particle simulations in conjunction with Space Weather Modeling. He is also investigating black hole accretion disks and associated jet generation using 3-D General Relativistic MHD codes.
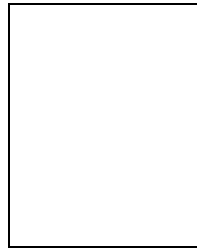
Shin-ichi Ohtani was born in Tokyo, Japan on February 6, 1962. He received B.S., M. S., and PhD degrees in geophysics from the University of Tokyo, Japan in 1984, 1986, and 1989. For a thesis study he investigated field-aligned currents in the magnetotail with satellite magnetic field data. He was a postdoctoral fellow of the Japanese Society for the Promotion of Science for Japanese Junior Scientists at the University of Tokyo from 1989 to 1991. He was a visiting scientist at the Johns Hopkins University Applied Physics Laboratory (JHU/APL) in 1990 and joined JHU/APL as a postdoctoral fellow in 1991. He has been a senior professional staff member since 1994. He has studied various magnetospheric phenomena with satellite observations. The list of his research topics includes dayside field-aligned current systems, near-Earth substorm dynamics, and low-frequency magnetic pulsations.